Phys. Lett. B 869 (2025) 139855

Contents lists available at ScienceDirect

Physics Letters B

journal homepage: www.elsevier.com/locate/physletb

Letter

Exploring nuclear structure with multiparticle azimuthal correlations at the LHC

ALICE Collaboration[1,*]

European Organization for Nuclear Research, Geneve 23, CH-1211, Geneva, Switzerland

ARTICLE INFO

Editor: Dr. M. Doser

ABSTRACT

Details of the nuclear structure of ^{129}Xe, such as the quadrupole deformation and the nuclear diffuseness, are studied by extensive measurements of anisotropic-flow-related observables in Xe–Xe collisions at a centre-of-mass energy per nucleon pair $\sqrt{s_{\rm NN}} = 5.44$ TeV with the ALICE detector at the LHC. The results are compared with those from Pb–Pb collisions at $\sqrt{s_{\rm NN}} = 5.02$ TeV for a baseline, given that the ^{208}Pb nucleus exhibits a very weak deformation. Furthermore, comprehensive comparisons are performed with a state-of-the-art hybrid model using IP-Glasma + MUSIC + UrQMD. It is found that among various IP-Glasma + MUSIC + UrQMD calculations with different values of nuclear parameters, the one using a nuclear diffuseness parameter of $a_0 = 0.492$ and a nuclear quadrupole deformation parameter of $\beta_2 = 0.207$ provides a better description of the presented flow measurements. These studies represent the first systematic exploration of nuclear structure at TeV energies, utilizing a comprehensive set of anisotropic flow observables. The measurements serve as a critical experimental benchmark for rigorously testing the interplay between nuclear structure inputs and heavy-ion theoretical models.

1. Introduction

Over the past two decades, low-energy nuclear physics has made remarkable progress. Advancements in experimental methods such as laser spectroscopy and Coulomb excitation techniques reveal additional insights into the size and shape of atomic nuclei [1–6]. On the theoretical side, the advent of *ab-initio* methods has allowed the description of light and medium-mass nuclei from first principles [7–11] and a flagship calculation of ^{208}Pb has been recently reported [12]. Nevertheless, systematic calculations of heavy-mass systems are still not yet possible, in particular, due to the computational difficulty in handling the (necessary) three-body nuclear interaction in large model spaces [13]. Recent studies in high-energy heavy-ion collisions at the Relativistic Heavy-Ion Collider (RHIC) [14–18] and the Large Hadron Collider (LHC) [19–23] have demonstrated that nuclear collisions at ultrarelativistic energies offer promising new approaches for nuclear structure studies. These studies successfully probed the nuclear shape from light to heavy nuclei [16–18,24–29] and the neutron skin of ^{208}Pb, ^{96}Zr, and ^{96}Ru [30,31]. Among these experimental approaches, anisotropic flow phenomena have been found to carry the imaging power of the nuclear structures at relativistic energies [16,24,32–38]. Anisotropic flow, which quantifies the anisotropic azimuthal distribution of the momenta of the produced particles, reflects the initial geometry and fluctuations of the overlapping region and probes the shape (or structure) of the colliding nuclei [39–44]. The anisotropic flow is characterised by the Fourier expansion of the azimuthal distribution of produced particles [45]

$$\frac{dN}{d\varphi} \propto 1 + 2\sum_{n=1}^{\infty} v_n \cos[n(\varphi - \Psi_n)], \quad (1)$$

where φ is the azimuthal angle of particle momentum and Ψ_n is the $n^{\rm th}$-order symmetry plane. The coefficients v_n are called flow coefficients and can be calculated as

$$v_n = \langle \cos[n(\varphi - \Psi_n)] \rangle. \quad (2)$$

Here, the brackets $\langle\rangle$ denote an average over all particles in one event. With v_n and Ψ_n, the n$^{\rm th}$ order (complex) anisotropic flow V_n are defined as

$$V_n \equiv v_n e^{in\Psi_n}. \quad (3)$$

Systematic measurements of v_n [14,19,23,46–51], event-by-event flow fluctuations [52–57], and correlations between various flow coefficients [58–63] enabled the extraction of the transport properties of the Quark-Gluon Plasma (QGP) and to constrain the initial conditions of the heavy-ion collisions [64]. It has been shown that the low-harmonic flow coefficients are linearly correlated with the initial eccentricity coefficients of the same order [65,66] and that the higher harmonic flow

* Corresponding author.
E-mail address: alice-publications@cern.ch

[1] See Appendix B for the list of collaboration members.

https://doi.org/10.1016/j.physletb.2025.139855
Received 19 September 2024; Received in revised form 18 July 2025; Accepted 27 August 2025
Available online 1 September 2025
0370-2693/

coefficients, in particular their nonlinear flow mode, carry information about the correlations between different participant planes [59,61]. Furthermore, the correlation between v_2 and v_3, characterised by normalised symmetric cumulants NSC(3, 2) [67], has been found to reflect correlation between ε_2 and ε_3 eccentricity coefficients [58,62,68]. These observables are widely recognised as powerful tools for precisely constraining the initial conditions of relativistic heavy-ion collisions [44].

For the initial state of heavy-ion collisions, the nuclear density profile $\rho(r, \theta, \phi)$ of the colliding nuclei can be described by the Woods–Saxon distribution [34,69]

$$\rho(r, \theta, \phi) = \frac{\rho_0}{1 + e^{[r - R(\theta,\phi)]/a_0}}, \tag{4}$$

where r, θ, and ϕ define the position of a nucleon presented in spherical coordinates, of which the origin is the centre of the nucleus. The constant ρ_0 ensures that the integral of the distribution corresponds to the number of nucleons in the nucleus. The a_0 parameter represents the nuclear diffuseness. The $R(\theta, \phi) = R_0(1 + \beta_2[\cos\gamma Y_{2,0} + \sin\gamma Y_{2,2}])$ term models the nuclear surface expanded in terms of spherical harmonics $Y_{n,m}$, keeping terms up to $n = 2$ that are the most relevant in the structure of ^{129}Xe [20,27,33]. Notably, $Y_{2,-2}$, $Y_{2,-1}$, and $Y_{2,1}$ are utilised to establish the intrinsic frame, which renders $Y_{2,0}$ and $Y_{2,2}$ as the only pertinent degrees of freedom. In $R(\theta, \phi)$, R_0 denotes the nuclear radius, and β_2 is the quadrupole deformation parameter. In low-energy nuclear experiments, β_2 for even-A isotopes of Xe can be extracted using the electric quadrupole transition probability B(E2)↑ from the ground 0^+ to the first-excited 2^+ state [70,71], although such extraction can be deficient by approximately 20 % due to fragmentation of the low-lying electric-quadrupole strength [72]. By interpolating the values between ^{128}Xe and ^{130}Xe, β_2 for ^{129}Xe was estimated to be 0.18 ± 0.02 [20]. Finally, the triaxial parameter γ reflects the inequality of the axes of the spheroid.

As described flow observables effectively capture a snapshot of the initial geometry of the collision and, by extension, offer a glimpse into the structure of the colliding nuclei, such as quadrupole deformation and triaxial structure. This "imaging power" of complex flow observables has been validated in recent theoretical model calculations and has shown great promise [25,27,29,33,37,38]. A systematic study of various anisotropic flow observables is essential for investigating nuclear structure at ultrarelativistic energies. Nevertheless, only simple flow observables involving fewer particle correlations, such as v_n coefficients, have been measured and used for studying nuclear structure [17,19]. The remaining, more complex flow observables, which involve multi-particle correlations and are likely more sensitive to the structure of the colliding nuclei [37,73], have not yet been explored experimentally.

This Letter presents systematic measurements of a comprehensive set of flow observables using charged particles from Xe–Xe collisions at a centre-of-mass energy per nucleon pair $\sqrt{s_{\mathrm{NN}}}$ = 5.44 TeV recorded by the ALICE detector, representing their first application to probe nuclear structure in heavy-ion collisions. In addition, the corresponding measurements from Pb–Pb collisions at $\sqrt{s_{\mathrm{NN}}}$ = 5.02 TeV , which provide a baseline because of the near-spherical shape of ^{208}Pb [70], are shown. Observables used in this study, including flow coefficients, flow fluctuations, nonlinear flow modes, and correlations between flow coefficients, are introduced in Section 2. Section 3 presents the experimental setup and the evaluation of systematical uncertainties. The results are discussed in Section 4, followed by the summary in Section 5.

2. Observables and analysis method

Flow coefficients v_n are usually measured by using two and four-particle cumulants [67,74–76]

$$\begin{aligned} v_n\{2\} &\equiv \sqrt{c_n\{2\}}, \\ v_n\{4\} &\equiv \sqrt[4]{-c_n\{4\}}, \end{aligned} \tag{5}$$

where $c_n\{2\}$ and $c_n\{4\}$ are the two and four-particle cumulants, respectively. It is known that $v_n\{2\}$ and $v_n\{4\}$ carry opposite contributions from flow fluctuations to the cumulant estimates [77]. When non-flow effects, which are the azimuthal angle correlations not associated with the symmetry plane, are small, the flow coefficients can be split into mean flow and flow fluctuation according to

$$\begin{aligned} v_n\{2\}^2 &\approx \langle v_n\rangle^2 + \sigma_{v_n}^2, \\ v_n\{4\}^2 &\approx \langle v_n\rangle^2 - \sigma_{v_n}^2. \end{aligned} \tag{6}$$

Here σ_{v_n} is the standard deviation of the v_n distribution, known as event-by-event fluctuation of v_n, and $\langle v_n\rangle$ is the mean value of the v_n distribution.

For $n = 2$ and $n = 3$, v_n coefficients for central and midcentral collisions are linearly correlated with the initial anisotropy coefficients ε_n [65,66], where ε_n is determined from the initial energy density profile [78]

$$\varepsilon_n e^{in\Phi_n} = -\frac{\langle r^n e^{in\phi}\rangle}{\langle r^n\rangle} \ (n > 1), \tag{7}$$

where $\langle\rangle$ represents an average among the transverse positions (r, ϕ) of all participating nucleons, with ϕ representing the azimuthal angle and r characterising the radial distance from the origin of the system. The Φ_n angle defines the symmetry plane of participant nucleons in the initial conditions. Recent studies have shown that nuclear quadrupole deformation strongly affects the initial eccentricity, particularly in the most central collisions [16,24,34]. Therefore, the final state v_n is expected to be a powerful tool to probe the deformations.

The high order flow coefficients v_n $(n > 3)$ receive contributions not only from the linear response to the initial ε_n but also from the nonlinear response originated from lower order ε_2 and/or ε_3 [79–81]. For example, the 4$^{\text{th}}$ order (complex) anisotropic flow V_4 can be decomposed into linear (V_4^{L}) and nonlinear (V_4^{NL}) components according to

$$V_4 = V_4^{\mathrm{L}} + V_4^{\mathrm{NL}}, \tag{8}$$

whose magnitudes are denoted by v_4^{L} and $v_{4,22}$, respectively. The subscript of $v_{4,22}$ represents the part of v_4 coming from ε_2^2 [79–81]. In Eq. (8) V_4^{L} and V_4^{NL} are considered to be uncorrelated and $v_{4,22}$ can be measured via a projection of V_4 onto the direction of V_2 [59,81]

$$v_{4,22} = \frac{\Re\langle V_4 (V_2^*)^2\rangle}{\sqrt{\langle |V_2|^4\rangle}}. \tag{9}$$

The magnitude of the linear component can be easily derived as $v_4^{\mathrm{L}} = \sqrt{v_4^2\{2\} - v_{4,22}^2}$.

Furthermore, the correlation between the symmetry planes Ψ_4 and Ψ_2 can be probed via the nonlinear flow correlation $\rho_{4,22}$ proposed in Ref. [81]. It is defined by the ratio of $v_{4,22}$ and $v_4\{2\}$

$$\rho_{4,22} = \frac{v_{4,22}}{v_4\{2\}} \approx \langle\cos(4\Psi_4 - 4\Psi_2)\rangle. \tag{10}$$

In addition, the nonlinear component V_4^{NL} can be further decomposed as

$$\begin{aligned} V_4^{\mathrm{NL}} &\approx \chi_{4,22}(V_2)^2, \\ \chi_{4,22} &= \frac{v_{4,22}}{\sqrt{\langle |V_2|^4\rangle}} = \frac{\Re\langle V_4 (V_2^*)^2\rangle}{\langle |V_2|^4\rangle}, \end{aligned} \tag{11}$$

where $\chi_{4,22}$ is called the nonlinear flow-mode coefficient. It represents the strength of nonlinear response to V_4 and is independent of ε_2. Recent studies with both transport and hydrodynamic model calculations have shown that nonlinear flow mode observables such as $v_{4,22}$, $\rho_{4,22}$, and $\chi_{4,22}$, owing to their different sensitivities to different stages of heavy-ion collisions [64,67,79,82–84], bring distinction power to the study of deformation of the colliding nuclei [25,35,37].

All the observables measured in this study are based on two- and multiparticle correlations, which can be obtained using the *Generic Framework* [67,76,85] for flow studies. To suppress non-flow contributions, a pseudorapidity gap $|\Delta\eta| > 1.0$ was applied in the two-particle correlations in the second harmonic. For high order ($n \geq 3$) correlations, a looser pseudorapidity gap of $|\Delta\eta| > 0.8$ was applied to preserve more particles for the analysis, considering the limited size of the Xe–Xe data sample. For the multiparticle correlations, which are less sensitive to non-flow contaminations, $|\Delta\eta| > 0.8$ was also applied, except for $v_2\{4\}$, where the pseudorapidity gap is unnecessary as their potential non-flow effects are negligible [76,86].

Except $v_2\{2\}$, $v_3\{2\}$, $v_4\{2\}$, and $v_2\{4\}$, which are taken from Ref. [19], the other observables are measured for the first time in Xe–Xe collisions. For Pb–Pb collisions, measurements of most observables were significantly improved after using the entire Run 2 data compared with previous measurements based only on the 2015 data sample [47,52,61,62].

3. Analysis details

The data sample analysed in this study was recorded by the ALICE detector [87–90] during the Xe–Xe run at $\sqrt{s_{\rm NN}} = 5.44$ TeV in 2017 and Pb–Pb runs at $\sqrt{s_{\rm NN}} = 5.02$ TeV in 2015 and 2018 at the LHC. Minimum bias events were triggered by the coincidence of two scintillator counter arrays, V0A and V0C [87,91], covering the pseudorapidity intervals $2.8 < \eta < 5.1$ and $-3.7 < \eta < -1.7$, respectively. Additional Pb–Pb events in the 0–10 % and 30–50 % centrality classes were recorded in 2018, using central and semicentral triggers, respectively, to maximise the integrated luminosity for central and semiperipheral collisions. Pile-up events, where multiple collisions are included in one single event, were rejected using the timing information from the V0 detectors and selections on the correlation of the multiplicity measured by the Inner Tracking System (ITS) [87,92] and the Time Projection Chamber (TPC) [87,93]. Charged particles are reconstructed in the central pseudorapidity region from their hits in the ITS, which is composed of six layers of silicon detectors surrounding the beam vacuum tube, and their energy deposits in the TPC. The track reconstruction in the ITS and the TPC provided the information on the primary vertex. The position of the primary vertex along the beam direction, V_z, was required to be within ± 10 cm from the centre of the detector. The analysis was performed as a function of collision centrality, determined using the information from the V0 detectors [20,94] and expressed as percentiles of the total inelastic Xe–Xe or Pb–Pb cross sections. The whole centrality range considered in this analysis was 0–60 %, where 0 % corresponds to the most central collisions. After the event selection, about 0.8 million Xe–Xe events and 163 million Pb–Pb events were analysed in this work.

Charged-particle tracks in the pseudorapidity region $|\eta| < 0.8$ and transverse momentum region $0.2 < p_{\rm T} < 3.0$ GeV/c were selected for the analysis. The track quality was ensured by requiring at least 70 TPC space points out of a maximum of 159 with an average χ^2 per degree of freedom of the track fit lower than 2.5. The distance of the closest approach (DCA) to the primary vertex in the beam direction, DCA$_z$, was required to be less than 2 cm. In addition, the DCA in the transverse plane was required to be DCA$_{xy} < 0.0105 + 0.0350 p_{\rm T}^{-1.1}$ cm, with $p_{\rm T}$ measured in GeV/c, which gives a $p_{\rm T}$-dependent selection on DCA$_{xy}$ with thresholds at 0.22 cm at 0.2 GeV/c and 0.02 cm at 3.0 GeV/c. A $p_{\rm T}$-dependent weight obtained from simulations performed with the HIJING event generator [95,96] combined with the GEANT3 transport code [97] was applied to correct for the track reconstruction efficiency. The track reconstruction efficiency ranges from 62 % to 80 % for $p_{\rm T} < 1.0$ GeV/c and drops slightly for higher $p_{\rm T}$ reaching a roughly constant value of about 76 %. In addition, φ distributions of the reconstructed tracks were utilised for extracting a non-uniform acceptance correction.

The sources of systematic uncertainty have been investigated by varying the criteria for selecting events and tracks. For event selections, the requirement for primary vertex position from the centre of the detector V_z was varied to ±5, ±7, and ±9 cm, respectively. In addition, the centrality estimation was alternatively determined by using the number of hits in the second-most internal layer of the ITS. In general, these sources yield uncertainties below 1 %; except the uncertainties associated with centrality estimation for $v_{4,22}$, $\rho_{4,22}$, and $\chi_{4,22}$ whose maximum levels reached 1 %. Furthermore, the systematic effect from pile-up events was studied by varying the selections on the correlations between multiplicities from the ITS and the TPC being found negligible.

Similarly, for the track selections, the minimum number of TPC space points was varied to 80, 90, and 100. The requirement for DCA$_{xy}$ was changed to DCA$_{xy} < 0.0090 + 0.0300 p_{\rm T}^{-1.1}$ cm, with $p_{\rm T}$ measured in GeV/c, while DCA$_z$ was required to be within 1.0 or 0.5 cm. These sources typically result in uncertainties of less than 1 %. Finally, the systematic uncertainties that were statistically significant according to the recommendation in Ref. [98] were added in quadrature to obtain the total systematic uncertainty. The total systematic uncertainties are typically less than 2 % in the 0–60 % centrality range, and they are denoted as grey boxes in the figures in Section 4.

4. Results

Fig. 1 presents the measurements of $v_2\{m\}(m = 2, 4)$ in Xe–Xe and Pb–Pb collisions as a function of centrality. In the upper panels, $v_2\{2, |\Delta\eta| > 1.0\}$ and $v_2\{4\}$ are shown. They increase from central to peripheral Xe–Xe and Pb–Pb collisions. The comparisons between Xe–Xe and Pb–Pb results are quantified as ratios in the bottom panels. Considering the similar dynamic evolution of the created matter in Pb–Pb and Xe–Xe collisions, the ratios of flow observables should largely cancel the final state effects and thus mainly reflect the information on the initial conditions, including the nuclear structure. This has been validated in recent hydrodynamic and transport model calculations [37,101]. Both $v_2\{2, |\Delta\eta| > 1.0\}$ and $v_2\{4\}$ ratios decrease steeply with increasing centrality percentile in central collisions and then level off for midcentral collisions. The $v_2\{2, |\Delta\eta| > 1.0\}$ ratio starts at approximately 1.5 in the most central collisions and is larger than unity in the centrality range 0–15 %, whereas the $v_2\{4\}$ ratio starts at approximately 1.3 and is above unity only in the 5 % most central collisions. In a central collision, the fluctuations of the overlap region play a dominant role, and smaller system size (Xe–Xe collisions) generates stronger fluctuations [102], which causes both ratios to be larger than unity. In addition, the deformation of ^{129}Xe nuclei further enhances ε_2 in ultracentral collisions of 0–5 % centrality; this effect will be discussed in detail later. In midcentral collisions, $v_2\{2, |\Delta\eta| > 1.0\}$ and $v_2\{4\}$ ratios remain at approximately 0.9 and 0.85, respectively. The ratios are below unity due to viscous effects during the medium expansion [19,103,104].

Unlike previous studies [27,38,105] that investigated nuclear structure based solely on initial-state estimates, the presented measurements are compared with calculations using the sequential combination of the impact-parameter Glasma (IP-Glasma) initial conditions, the MUSIC relativistic hydrodynamic model, and the ultrarelativistic quantum molecular dynamics (UrQMD) model for hadronic rescatterings. This hybrid model is denoted as IP-Glasma + MUSIC + UrQMD [99,100]. These calculations are presented as bands of different colours, where the thickness of bands denote the statistical uncertainties of the calculations. The IP-Glasma + MUSIC + UrQMD model has successfully described particle production and complex anisotropic flow measurements in Pb–Pb collisions at the LHC [99], providing valuable insights into both the initial conditions and the dynamical evolution of colliding systems. To investigate the impact of nuclear structure, different initial conditions were used for Xe–Xe calculations, varying the β_2 quadrupole deformation and the a_0 nuclear diffuseness. The values of β_2 and a_0 were adopted based on existing predictions. Specifically, $a_0 = 0.492$ and $\beta_2 = 0.207$ are taken from Ref. [27], $\beta_2 = 0.162$ is from Ref. [106], and $a_0 = 0.57$ is used in Ref. [107]. Notably, the setting of $\beta_2 = 0$ represents a special scenario of a spherical nucleus. Despite the ongoing investigation into the nuclear shape phase transition of ^{129}Xe, where the γ-soft structure was discussed [38], the current calculations set the γ parameter to zero, as all the presented flow observables have been found to be insensitive to the triaxial structure [37]. For Pb–Pb calculations, a very

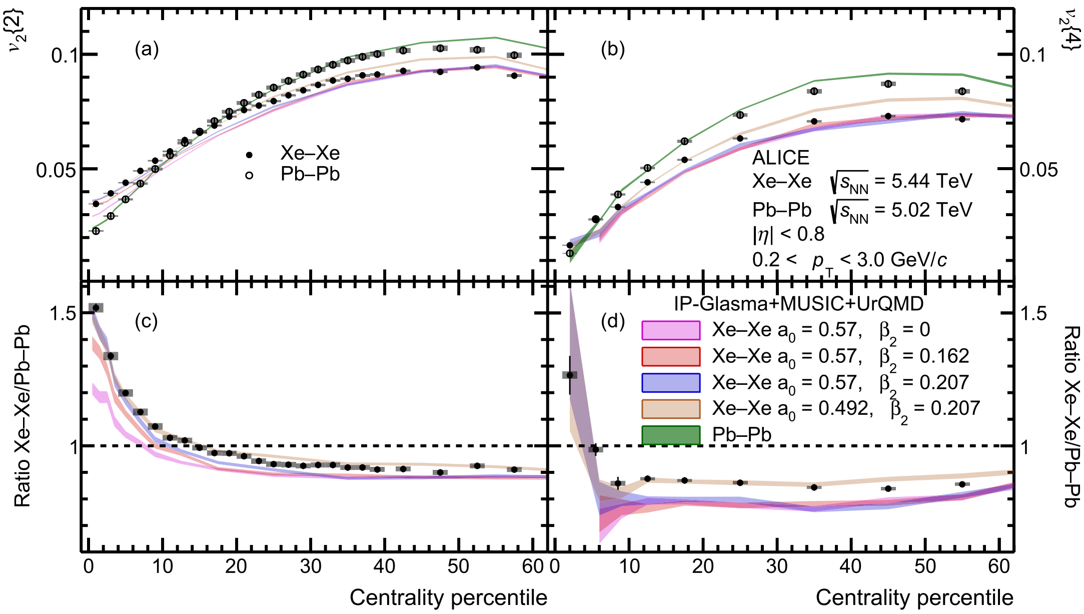

Fig. 1. Panels (a) and (b): Charged particle $v_2\{2, |\Delta\eta| > 1.0\}$ (left) and $v_2\{4\}$ (right) as a function of centrality in Xe–Xe and Pb–Pb collisions at $\sqrt{s_{NN}}$ = 5.44 TeV and $\sqrt{s_{NN}}$ = 5.02 TeV , respectively. Panels (c) and (d): Ratio between Xe–Xe and Pb–Pb $v_2\{2, |\Delta\eta| > 1.0\}$ (left) and $v_2\{4\}$ (right). Statistical and systematical uncertainties are shown as vertical lines and grey boxes, respectively. The measurements are compared with IP-Glasma + MUSIC + UrQMD calculations [99,100] to constrain the β_2 and a_0 parameters of ^{129}Xe nuclei. The thickness of the bands represent statistical uncertainties.

weak deformation $\beta_2 = 0.055$ of ^{208}Pb is adopted [71], which is also used in Ref. [27] when the ultra-relativistic energy is considered. In Fig. 1, the IP-Glasma + MUSIC + UrQMD calculations in Pb–Pb collisions (green bands) align well with the measurements of $v_2\{2, |\Delta\eta| > 1.0\}$ and $v_2\{4\}$ up to a centrality of 35 %. However, beyond 35 % centrality, the calculated values exceed the measurements. For Xe–Xe , in the 0–15 % centrality range, the calculations with $a_0 = 0.57, \beta_2 = 0.207$ (blue bands) and $a_0 = 0.492, \beta_2 = 0.207$ (brown bands) match the measurements of $v_2\{2, |\Delta\eta| > 1.0\}$ better, while they underestimate $v_2\{4\}$ in 5–10 % centrality. Then for the 15–25 % centrality range, the measurements of $v_2\{2, |\Delta\eta| > 1.0\}$ and $v_2\{4\}$ are better described by the calculations when the parameters are set to $a_0 = 0.492, \beta_2 = 0.207$ (brown bands). Furthermore, in the 35–60 % centrality range, the calculations with $a_0 = 0.57, \beta_2 = 0.207$ (blue bands), as well as $a_0 = 0.57, \beta_2 = 0.162$ (red bands) and $a_0 = 0.57, \beta_2 = 0$ (pink bands) provide better descriptions for the measurements of both $v_2\{2, |\Delta\eta| > 1.0\}$ and $v_2\{4\}$. Notably in the 0–10 % centrality range in Fig. 1(c), the calculations for $v_2\{2, |\Delta\eta| > 1.0\}$ with $a_0 = 0.57, \beta_2 = 0.162$ and $a_0 = 0.57, \beta_2 = 0$ are approximately 5 % and 20 % lower, respectively, than the measured ratios of Xe–Xe and Pb–Pb results. This discrepancy highlights the contributions from the quadrupole deformation of ^{129}Xe [24,25,34,35,37]. In this centrality range, the initial shape of the overlapping region is primarily determined by the shape of the colliding nuclei; thus, the deformed nuclei enhance the initial eccentricity ε_2 of the overlapping region, consequently leading to larger v_2.

As introduced in Eq. (6), $v_2\{2\}$ and $v_2\{4\}$ receive contributions from both $\langle v_2\rangle$ and its event-by-event fluctuations σ_{v_2}. Consequently, mean flow and flow fluctuations can be measured separately using the combination of $v_2\{2\}$ and $v_2\{4\}$. Fig. 2 presents the centrality dependence of $\langle v_2\rangle$ and σ_{v_2} in Xe–Xe and Pb–Pb collisions. In panel (a), $\langle v_2\rangle$ increases from central to peripheral collisions for both Xe–Xe and Pb–Pb collisions. The ratio between Xe–Xe and Pb–Pb $\langle v_2\rangle$ in panel (c) exceeds unity in 0–10 % centrality, then decreases to approximately 0.9 in the midcentral collisions. Overall, σ_{v_2} in Xe–Xe is larger than in Pb–Pb in the 0–60 % centrality range, attributable to the smaller system size of Xe–Xe collisions [102]. The ratio between Xe-Xe and Pb-Pb σ_{v_2} in panel (d) starts at approximately 1.5 in the most central collisions and steadily decreases with increasing centrality percentile, converging to unity at 60 % centrality. For $\langle v_2\rangle$ in Fig. 2(a) and (c), the IP-Glasma + MUSIC + UrQMD calculations with $\beta_2 = 0.207$ describe the measurements in 0–10 % centrality. Due to the extensive statistical samples required, other calculations are only available for centralities above 5 %, which notably underestimate the measured $\langle v_2\rangle$ for the 0–20 % centrality range. For σ_{v_2} shown in Fig. 2(b) and (d), most calculations describe the measurements within the presented centrality range, except for the one with $a_0 = 0.57$ and $\beta_2 = 0$, which falls below the measurement in 0–20 % centrality. A weaker elliptic flow fluctuation σ_{v_2} is seen in central Xe–Xe collisions when a spherical nuclear structure of ^{129}Xe is used in the model calculations. For centrality above 20 %, the calculations for σ_{v_2} with different a_0 and β_2 are compatible with each other within uncertainties, suggesting that σ_{v_2} might not depend on the nuclear diffuseness and deformation for non-central collisions.

In addition to the study of elliptic flow v_2 and its event-by-event fluctuations, the triangular flow $v_3\{2\}$ and quadrangular flow $v_4\{2\}$, which provide more precise constraints on the initial conditions [78,108], are also examined as a function of centrality in Fig. 3. In the upper panels, $v_3\{2, |\Delta\eta| > 0.8\}$ is notably larger in Xe–Xe than in Pb–Pb within the 0–35 % centrality range, while the $v_3\{2, |\Delta\eta| > 0.8\}$ measurements in Xe–Xe are smaller for more peripheral collisions. The $v_4\{2, |\Delta\eta| > 0.8\}$ results are compatible within uncertainties for both Xe–Xe and Pb–Pb collisions up to 30 % centrality, after which Xe–Xe results are smaller than those in Pb–Pb collisions. In the lower panels, accordingly, the ratios between Xe–Xe and Pb–Pb $v_3\{2, |\Delta\eta| > 0.8\}$ and $v_4\{2, |\Delta\eta| > 0.8\}$ decrease steadily with increasing centrality. The IP-Glasma + MUSIC + UrQMD calculations are lower than the $v_3\{2, |\Delta\eta| > 0.8\}$ measurements in Pb–Pb collisions up to 35 % centrality, beyond which the calculations overestimate the measurements. A similar pattern is observed for Xe–Xe collisions, where the calculations are roughly compatible with the $v_3\{2, |\Delta\eta| > 0.8\}$ measurements in the central collision and exceed the measured values for centrality above 20 %. Meanwhile, no difference is found among the $v_3\{2, |\Delta\eta| > 0.8\}$ calculations with different β_2 values. This is consistent with the expectation that $v_3\{2\}$, which is primarily driven by the linear response to the initial triangularity ε_3 [65,66], may be sensitive to octupole deformation β_3 but not to quadrupole deformation β_2. This has also been confirmed in the previous AMPT model studies [37]. Furthermore, for the Xe–Xe

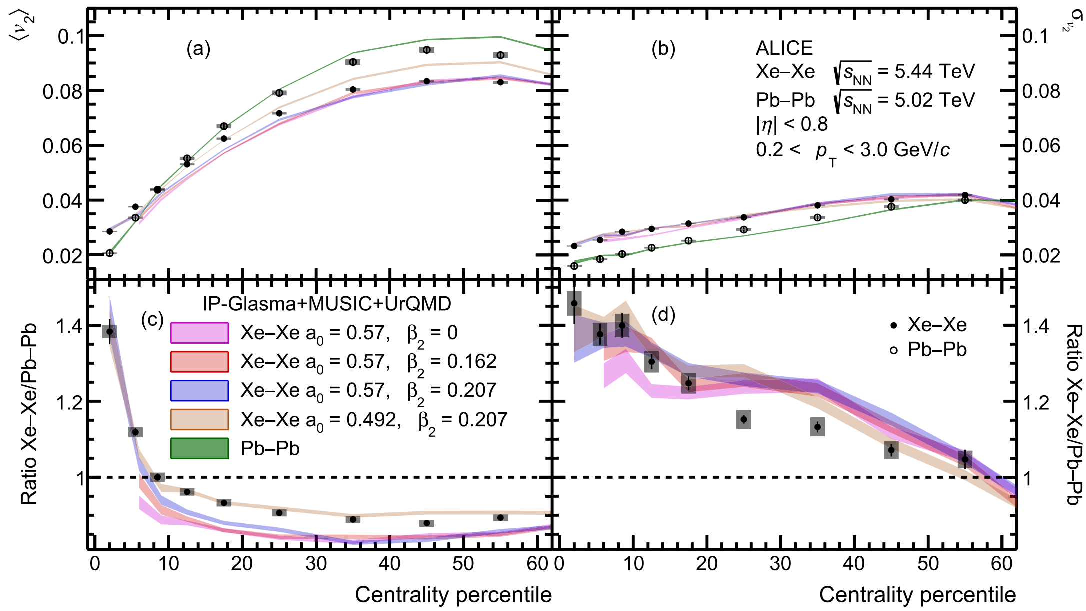

Fig. 2. Panels (a) and (b): Charged particle $\langle v_2 \rangle$ (left) and σ_{v_2} (right) as a function of centrality in Xe–Xe and Pb–Pb collisions at $\sqrt{s_{NN}}$ = 5.44 TeV and $\sqrt{s_{NN}}$ = 5.02 TeV , respectively. Panels (c) and (d): Ratio between Xe–Xe and Pb–Pb $\langle v_2 \rangle$ (left) and σ_{v_2} (right). Statistical and systematical uncertainties are shown as vertical lines and grey boxes, respectively. The measurements are compared with IP-Glasma + MUSIC + UrQMD calculations [99,100] to constrain the β_2 and a_0 parameters of ^{129}Xe nuclei. The thickness of the bands represent statistical uncertainties.

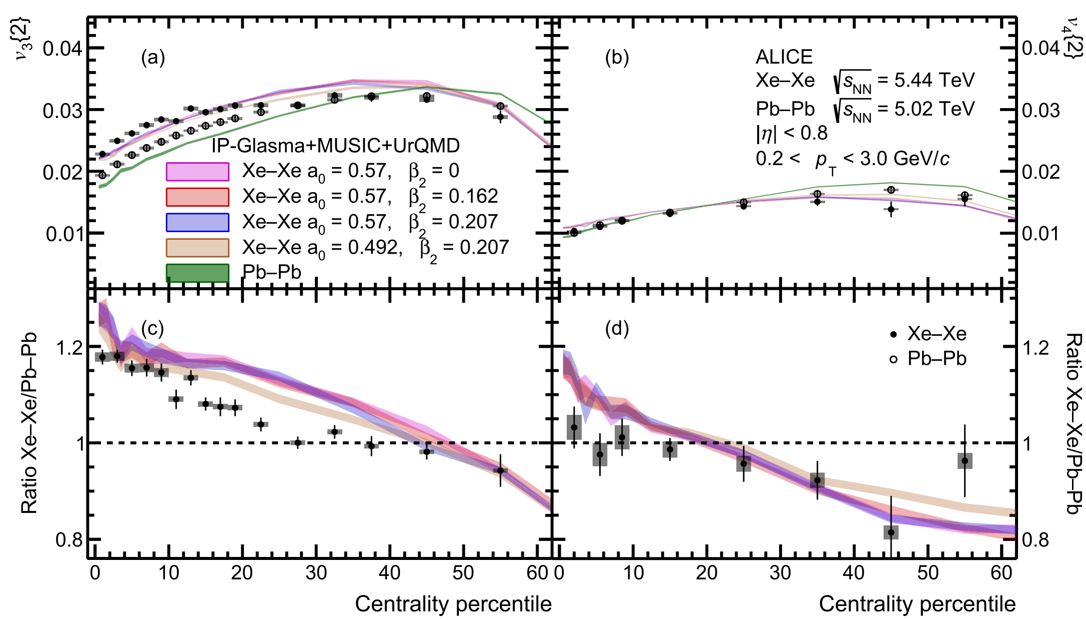

Fig. 3. Panels (a) and (b): Charged particle $v_3\{2, |\Delta\eta| > 0.8\}$ (left) and $v_4\{2, |\Delta\eta| > 0.8\}$ (right) as a function of centrality in Xe–Xe and Pb–Pb collisions at $\sqrt{s_{NN}}$ = 5.44 TeV and $\sqrt{s_{NN}}$ = 5.02 TeV , respectively. Panels (c) and (d): Ratio between Xe–Xe and Pb–Pb $v_3\{2, |\Delta\eta| > 0.8\}$ (left) and $v_4\{2, |\Delta\eta| > 0.8\}$ (right). Statistical and systematical uncertainties are shown as vertical lines and grey boxes, respectively. The measurements are compared with IP-Glasma + MUSIC + UrQMD calculations [99,100] to constrain the β_2 and a_0 parameters of ^{129}Xe nuclei. The thickness of the bands represent statistical uncertainties.

/Pb–Pb ratios in Fig. 3, the calculations qualitatively capture the general trend of the centrality dependence of the measured $v_3\{2, |\Delta\eta| > 0.8\}$ and $v_4\{2, |\Delta\eta| > 0.8\}$. However, all calculations for $v_3\{2, |\Delta\eta| > 0.8\}$ ratio are higher than the measurements in 10–40 % centrality. A distinction is observed between calculations from $a_0 = 0.57$ and $a_0 = 0.492$ in the 10–40 % centrality range; the latter exhibits a slightly better agreement with the measurement. Concurrently, the calculations appear to overestimate the $v_4\{2, |\Delta\eta| > 0.8\}$ ratio in central collisions. A difference between the calculations of $v_4\{2, |\Delta\eta| > 0.8\}$ with $a_0 = 0.57$ and $a_0 = 0.492$ is also noted in more peripheral collisions, as reported from previous AMPT calculations [35,37]. Unfortunately, the significant uncertainties in the measurements preclude a definitive conclusion as to which model calculation better reproduces them.

Fig. 4 shows the centrality dependence of the $v_{4,22}$ nonlinear flow modes Xe–Xe and Pb–Pb collisions. It has been established that $v_{4,22}$ exhibits considerable sensitivities to nuclear deformation parameters [37], originating from the initial ε_2^2. In the upper panels of Fig. 4, it can be seen that $v_{4,22}$ increases from central to peripheral Xe–Xe and Pb–Pb

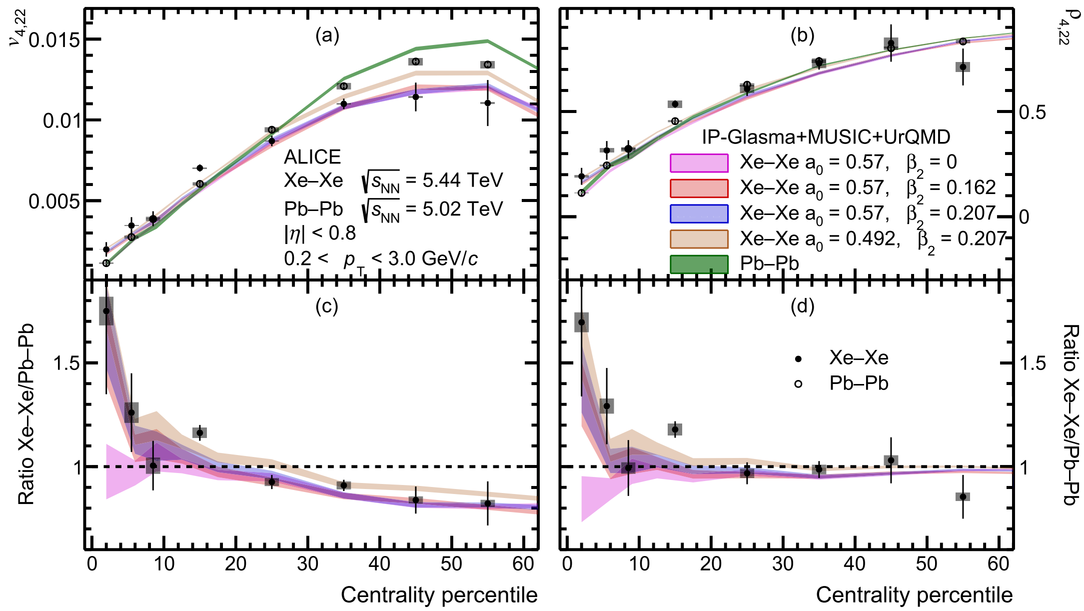

Fig. 4. Panels (a) and (b): Charged particle $v_{4,22}$ (left) and $\rho_{4,22}$ (right) as a function of centrality in Xe–Xe and Pb–Pb collisions at $\sqrt{s_{NN}}$ = 5.44 TeV and $\sqrt{s_{NN}}$ = 5.02 TeV , respectively. Panels (c) and (d): Ratio between Xe–Xe and Pb–Pb $v_{4,22}$ (left) and $\rho_{4,22}$ (right). Statistical and systematical uncertainties are shown as vertical lines and grey boxes, respectively. The measurements are compared with IP-Glasma + MUSIC + UrQMD calculations [99,100] to constrain the β_2 and a_0 parameters of ^{129}Xe nuclei. The thickness of the bands represent statistical uncertainties.

collisions. The $v_{4,22}$ ratio, shown in panel (c) of Fig. 4, starts at approximately 1.5 in most central collisions and decreases toward more peripheral collisions. In comparison to the measurements, the IP-Glasma + MUSIC + UrQMD calculations describe $v_{4,22}$ measurements in 0–35 % centrality and only marginally overestimate them in 35–60 % centrality for Pb–Pb collisions, while they quantitatively capture the $v_{4,22}$ measurements in Xe–Xe collisions. Regarding the ratios in Fig. 4(c), the measured $v_{4,22}$ ratios in the centrality range 0–20 % are better described by the IP-Glasma + MUSIC + UrQMD calculations with a non-zero β_2 and are significantly larger than the one with $\beta_2 = 0$. This aligns with expectations, as $v_{4,22}$ is primarily affected by ε_2^2 in central collisions [34] where ε_2 is influenced mainly by the nuclear quadrupole deformation β_2. Additionally, $v_{4,22}$ ratio calculations using $a_0 = 0.57$ describe the measurements in 20–60 % centrality better, whereas the one with $a_0 = 0.492$ overestimates the measured $v_{4,22}$ ratio. A similar observation on the sensitivity of $v_{4,22}$ to a_0 in midcentral collisions has been reported in the AMPT studies [37], suggesting that $v_{4,22}$ serves as a promising probe of the nuclear diffuseness.

In addition to the nonlinear flow modes, which depend on the magnitudes of v_2 and/or v_3, the symmetry plane correlation $\rho_{4,22}$ is investigated in Xe–Xe and Pb–Pb collisions. The $\rho_{4,22}$ has been identified as carrying unique sensitivities to the initial conditions of heavy-ion collisions, rendering it a valuable probe for the nuclear structure [59,61]. The measurements of $\rho_{4,22}$ are presented as a function of centrality in panels (b) and (d) of Fig. 4. In panel (b), $\rho_{4,22}$ shows an increase from central to peripheral collisions in both Xe–Xe and Pb–Pb collisions. The $\rho_{4,22}$ ratio drops steeply in the most central collisions, starting from approximately 1.7 down to unity for centralities above 20 %. Regarding the ratio of $\rho_{4,22}$ presented in panel (d), the IP-Glasma + MUSIC + UrQMD calculations offer a reasonable description of the measurements, except for the scenario with $\beta_2 = 0$ in the most central collisions, which assumes a spherical ^{129}Xe shape and misses the measured $\rho_{4,22}$ ratio. The pronounced correlations between second and fourth-order symmetry planes, Ψ_2 and Ψ_4, in Xe–Xe collision, are primarily ascribed to the shape of the colliding nuclei influencing the overlap region in central collisions. A deformed ^{129}Xe nuclear structure results in an elliptical overlapping region in central collisions, leading to preferred orientations for the symmetry planes rather than random fluctuations, thereby generating stronger correlations between Ψ_2 and Ψ_4 in Xe–Xe collisions than in Pb–Pb collisions. Overall, the IP-Glasma + MUSIC + UrQMD calculations, considering different a_0 values, do not exhibit significant differences in $\rho_{4,22}$, taking into account the considerable uncertainties in the model calculations.

Furthermore, the linear flow mode v_4^{L}, the nonlinear flow coefficient $\chi_{4,22}$, and NSC(3, 2) have been measured in Xe-Xe collisions at the LHC. These measurements are compared with model calculations of IP-Glasma + MUSIC + UrQMD, which reveal no sensitivity to the variations in nuclear structure. The relevant results are presented in Appendix A.

To quantify the agreement between the experimental measurements and the IP-Glasma + MUSIC + UrQMD model calculations with the different configurations, a χ^2/N_{dof} for each observable was calculated as

$$\chi^2/N_{dof} = \frac{1}{N_{dof}} \sum \frac{(y_i - f_i)^2}{\sigma_i^2}, \quad (12)$$

where y_i is the value of the observable experimental measurement at centrality range i and f_i is the value of the observable calculation for the same centrality range with the corresponding configuration, σ_i^2 is the quadratic sum of the statistical uncertainty σ_{stat}, systematic uncertainty σ_{sys}, and model uncertainty σ_{model}. The number of degrees of freedom N_{dof} is obtained by subtracting the number of parameters from the number of data points. Only the measured ratio (Xe–Xe /Pb–Pb) for each observable is considered. The χ^2/N_{dof} values for the observables considered in this work are shown in Fig. 5. Panel (a) restricts the centrality range to 0–20 %, and panel (b) restricts the centrality range to 20–60 %. The centrality region is separated because the β_2 parameter has a strong impact on the observables in central collisions, while the a_0 parameter shows influence across the 0–60 % centrality range. It can be seen that the IP-Glasma + MUSIC + UrQMD calculations with $\beta_2 = 0.207$ generally provide a better description of the measurements of v_2 related observables, as indicated by the smaller χ^2/N_{dof} values. In the 0–20 % centrality range, the calculations with $a_0 = 0.492, \beta_2 = 0.207$ yield the smallest χ^2/N_{dof} for $v_2\{2, |\Delta\eta| > 1.0\}$, $v_2\{4\}$ and $\langle v_2\rangle$, and result in a consistent χ^2/N_{dof} in comparison to the calculation using $a_0 = 0.57, \beta_2 = 0.207$ for σ_{v_2}. This shows the strong influences from β_2 and a_0 on those observables in central collisions. In the 20–60 % centrality range, the χ^2/N_{dof} results for v_2-related observables are similar for different β_2 values, indicating that the deformation effect is weak for non-central collisions. Meanwhile, the calculations with $a_0 = 0.492, \beta_2 = 0.207$ still provide the smallest χ^2/N_{dof} for $v_2\{2, |\Delta\eta| > 1.0\}$, $v_2\{4\}$ and $\langle v_2\rangle$,

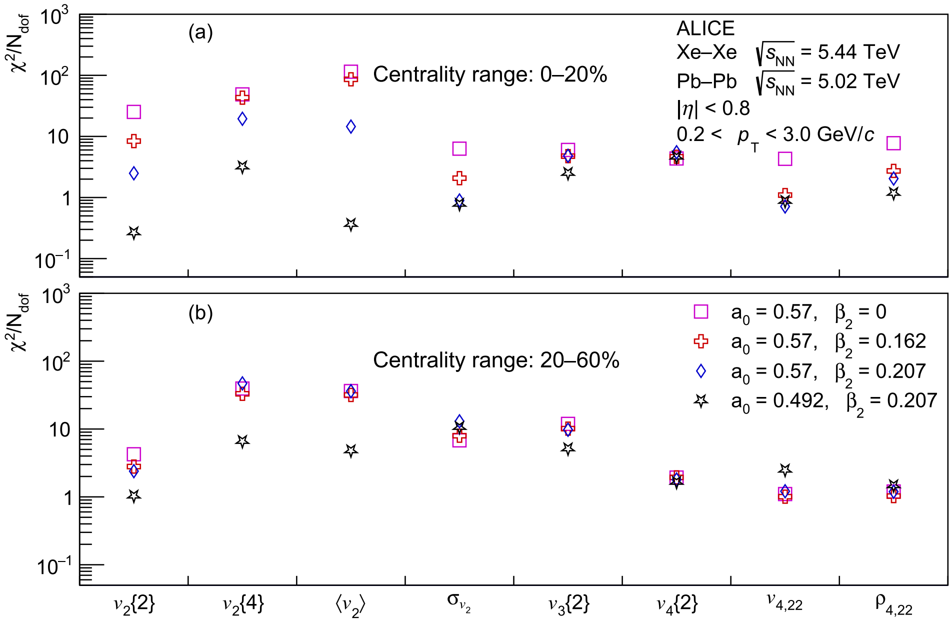

Fig. 5. Values of χ^2/N_{dof} between the measurements (Xe–Xe /Pb–Pb) and the calculations (Xe–Xe /Pb–Pb). The x-axis represents the different measured observables, and the y-axis is shown on a logarithmic scale. Panels (a) and (b) show the results for the 0–20 % and 20–60 % centrality ranges, respectively.

showing the influences from a_0 in midcentral collisions. In addition, the data-to-model χ^2/N_{dof} values are shown for the $v_3\{2,|\Delta\eta|>0.8\}$ and v_4 related observables. The IP-Glasma + MUSIC + UrQMD calculations with $a_0 = 0.492$ and $\beta_2 = 0.207$ provide better descriptions of $v_3\{2,|\Delta\eta|>0.8\}$, and they also perform reasonably well for $\rho_{4,22}$, compared to the calculations using different a_0 or β_2 parameters. In contrast, the calculations with $\beta_2 = 0$ consistently yield relatively poor descriptions, emphasising the significance of a finite quadrupole deformation for ^{129}Xe. For $v_4\{2,|\Delta\eta|>0.8\}$, all calculations exhibit similar χ^2/N_{dof} values, aligning with previous discussions that $v_4\{2,|\Delta\eta|>0.8\}$ is not sensitive to the variations in either a_0 or β_2. For $v_{4,22}$, calculations with $a_0 = 0.57$ yield smaller χ^2/N_{dof} values, which are influenced by the large uncertainties in both the model and the measurements. Overall, calculations with $a_0 = 0.492$ and $\beta_2 = 0.207$ align better with the measurements for the flow observables in Xe–Xe collisions.

It is noteworthy that the χ^2/N_{dof} test might not provide a precise measure but rather qualitatively reflects the potential sensitivities of flow observables to β_2 and a_0. It facilitates the initial exploration of how various flow observables respond to different nuclear structures. Notably, this approach was first applied in complex flow measurements in Pb–Pb collisions [61], introducing novel constraints on the tuning of the hydrodynamic framework with varying initial conditions. Subsequently, these flow measurements were incorporated into Global Bayesian fits, leading to the most precise constraints on Pb–Pb collisions initial conditions to date [64]. Therefore, the systematic measurements of complex flow observables presented in this paper are expected to be adopted soon in Bayesian fits, potentially enabling a more reliable extraction of nuclear structure parameters from relativistic nuclear collisions.

5. Summary

For the first time, measurements of complex flow observables through multiparticle azimuthal correlations have been employed to probe the nuclear structure in heavy-ion collisions. Systematic measurements of various flow observables, including anisotropic flow coefficients (v_n), flow fluctuations (σ_{v_2}), nonlinear and linear components of flow coefficients ($v_{4,22}$, v_4^{L}), nonlinear coefficients ($\chi_{4,22}$), correlations between different symmetry planes ($\rho_{4,22}$), and normalised symmetry cumulants have been performed in Xe–Xe and Pb–Pb collisions at $\sqrt{s_{NN}}$ = 5.44 TeV and 5.02 TeV, respectively. Notably, several flow observables exhibit pronounced differences in the ratio between Xe–Xe and Pb–Pb in the most central collisions, which are anticipated from the quadrupole deformation of the ^{129}Xe nuclear structure. Comprehensive comparisons between the experimental measurements and the IP-Glasma + MUSIC + UrQMD calculations are presented to quantify the effects of quadrupole deformation and nuclear diffuseness. Specifically, the calculations employing different β_2 quadrupole deformation parameters and a_0 nuclear diffuseness parameters are discussed. It has been found that among various IP-Glasma + MUSIC + UrQMD model calculations, the one using $\beta_2 = 0.207$ generally provides a better description of the flow measurements. Despite noticeable discrepancies between the measurements and the IP-Glasma + MUSIC + UrQMD predictions, the calculations using $a_0 = 0.492$ seem favoured by the presented measurements. Future Bayesian analysis will allow a more robust extraction of the β_2 and a_0 values. The distinct sensitivities of flow observables to β_2 and a_0 offer valuable insights into constraining the deformation and diffuseness of ^{129}Xe in its ground state. Systematic measurements of complex flow observables using multiparticle azimuthal correlations at the LHC are opening new avenues for investigating nuclear structure at the energy frontier, complementing low-energy nuclear structure studies and deepening the understanding of fundamental nuclear properties. Upcoming ^{16}O–^{16}O collisions at the LHC will provide novel opportunities to explore the full potential of the LHC on the nuclear structure study probing, in particular, for the first time the α-cluster structure of ^{16}O at the TeV energy scale [18,109–112].

Data availability

This manuscript has associated data in a HEPData repository at: https://www.hepdata.net/record/ins2825785.

Declaration of competing interest

The authors declare that they have no known competing financial interests or personal relationships that could have appeared to influence the work reported in this paper.

Acknowledgment

The ALICE Collaboration would like to thank Chun Shen and Bjoern Schenke for providing the latest calculations from the state-of-the-art models. The ALICE Collaboration would like to thank all its engineers and technicians for their invaluable contributions to the construction of the experiment and the CERN accelerator teams for the outstanding performance of the LHC complex. The ALICE Collaboration gratefully acknowledges the resources and support provided by all Grid centres and the Worldwide LHC Computing Grid (WLCG) collaboration. The ALICE Collaboration acknowledges the following funding agencies for their support in building and running the ALICE detector: A. I. Alikhanyan National Science Laboratory (Yerevan Physics Institute) Foundation (ANSL), State Committee of Science and World Federation of Scientists (WFS), Armenia; Austrian Academy of Sciences, Austrian Science Fund (FWF): [M 2467-N36] and Nationalstiftung für Forschung, Technologie und Entwicklung, Austria; Ministry of Communications and High Technologies, National Nuclear Research Center, Azerbaijan; Conselho Nacional de Desenvolvimento Científico e Tecnológico (CNPq), Financiadora de Estudos e Projetos (Finep), Fundação de Amparo à Pesquisa do Estado de São Paulo (FAPESP) and Universidade Federal do Rio Grande do Sul (UFRGS), Brazil; Bulgarian Ministry of Education and Science, within the National Roadmap for Research Infrastructures 2020–2027 (object CERN), Bulgaria; Ministry of Education of China (MOEC) , Ministry of Science & Technology of China (MSTC) and National Natural Science Foundation of China (NSFC), China; Ministry of Science and Education and Croatian Science Foundation, Croatia; Centro de Aplicaciones Tecnológicas y Desarrollo Nuclear (CEADEN), Cubaenergía, Cuba; Ministry of Education, Youth and Sports of the Czech Republic, Czech Republic; The Danish Council for Independent Research | Natural Sciences, the VILLUM FONDEN and Danish National Research Foundation (DNRF), Denmark; Helsinki Institute of Physics (HIP), Finland; Commissariat à l'Energie Atomique (CEA) and Institut National de Physique Nucléaire et de Physique des Particules (IN2P3) and Centre National de la Recherche Scientifique (CNRS), France; Bundesministerium für Bildung und Forschung (BMBF) and GSI Helmholtzzentrum für Schwerionenforschung GmbH, Germany; General Secretariat for Research and Technology, Ministry of Education, Research and Religions, Greece; National Research, Development and Innovation Office, Hungary; Department of Atomic Energy Government of India (DAE), Department of Science and Technology, Government of India (DST), University Grants Commission, Government of India (UGC) and Council of Scientific and Industrial Research (CSIR), India; National Research and Innovation Agency - BRIN, Indonesia; Istituto Nazionale di Fisica Nucleare (INFN), Italy; Japanese Ministry of Education, Culture, Sports, Science and Technology (MEXT) and Japan Society for the Promotion of Science (JSPS) KAKENHI, Japan; Consejo Nacional de Ciencia (CONACYT) y Tecnología, through Fondo de Cooperación Internacional en Ciencia y Tecnología (FONCICYT) and Dirección General de Asuntos del Personal Academico (DGAPA), Mexico; Nederlandse Organisatie voor Wetenschappelijk Onderzoek (NWO), Netherlands; The Research Council of Norway, Norway; Pontificia Universidad Católica del Perú, Peru; Ministry of Science and Higher Education, National Science Centre and WUT ID-UB, Poland; Korea Institute of Science and Technology Information and National Research Foundation of Korea (NRF), Republic of Korea; Ministry of Education and Scientific Research, Institute of Atomic Physics, Ministry of Research and Innovation and Institute of Atomic Physics and Universitatea Nationala de Stiinta si Tehnologie Politehnica Bucuresti, Romania; Ministry of Education, Science, Research and Sport of the Slovak Republic, Slovakia; National Research Foundation of South Africa, South Africa; Swedish Research Council (VR) and Knut & Alice Wallenberg Foundation (KAW), Sweden; European Organization for Nuclear Research, Switzerland; Suranaree University of Technology (SUT), National Science and Technology Development Agency (NSTDA) and National Science, Research and Innovation Fund (NSRF via PMU-B B05F650021), Thailand; Turkish Energy, Nuclear and Mineral Research Agency (TENMAK), Turkey; National Academy of Sciences of Ukraine, Ukraine; Science and Technology Facilities Council (STFC), United Kingdom; National Science Foundation of the United States of America (NSF) and United States Department of Energy, Office of Nuclear Physics (DOE NP), United States of America. In addition, individual groups or members have received support from: Czech Science Foundation (grant no. 23-07499S), Czech Republic; FORTE project, reg. no. CZ.02.01.01/00/22_008/0004632, Czech Republic, co-funded by the European Union, Czech Republic; European Research Council (grant no. 950692), European Union; ICSC - Centro Nazionale di Ricerca in High Performance Computing, Big Data and Quantum Computing, European Union - NextGenerationEU; Academy of Finland (Center of Excellence in Quark Matter) (grant nos. 346327, 346328), Finland; Deutsche Forschungs Gemeinschaft (DFG, German Research Foundation) "Neutrinos and Dark Matter in Astro- and Particle Physics" (grant no. SFB 1258), Germany.

Supplementary material

Supplementary material associated with this article can be found in the online version at 10.1016/j.physletb.2025.139855.

Appendix B. The ALICE Collaboration

S. Acharya [127], A. Agarwal[135], G. Aglieri Rinella [32], L. Aglietta [24], M. Agnello [29], N. Agrawal [25], Z. Ahammed [135], S. Ahmad [15], S.U. Ahn [71], I. Ahuja [36], A. Akindinov [141], V. Akishina[38], M. Al-Turany [97], D. Aleksandrov [141], B. Alessandro [56], H.M. Alfanda [6], R. Alfaro Molina [67], B. Ali [15], A. Alici [25], N. Alizadehvandchali [116], A. Alkin [104], J. Alme [20], G. Alocco [24,52], T. Alt [64], A.R. Altamura [50], I. Altsybeev [95], J.R. Alvarado [44], M.N. Anaam [6], C. Andrei [45], N. Andreou [115], A. Andronic [126], E. Andronov [141], V. Anguelov [94], F. Antinori [54], P. Antonioli [51], N. Apadula [74], L. Aphecetche [103], H. Appelshäuser [64], C. Arata [73], S. Arcelli [25], R. Arnaldi [56], J.G.M.C.A. Arneiro [110], I.C. Arsene [19], M. Arslandok [138], A. Augustinus [32], R. Averbeck [97], D. Averyanov [141], M.D. Azmi [15], H. Baba[124], A. Badalà [53], J. Bae [104], Y.W. Baek [40], X. Bai [120], R. Bailhache [64], Y. Bailung [48], R. Bala [91], A. Balbino [29], A. Baldisseri [130], B. Balis [2], Z. Banoo [91], V. Barbasova [36], F. Barile [31], L. Barioglio [56], M. Barlou [78], B. Barman [41], G.G. Barnaföldi [46], L.S. Barnby [115], E. Barreau [103], V. Barret [127], L. Barreto [110], C. Bartels [119], K. Barth [32], E. Bartsch [64], N. Bastid [127], S. Basu [75], G. Batigne [103], D. Battistini [95], B. Batyunya [142], D. Bauri[47], J.L. Bazo Alba [101], I.G. Bearden [83], C. Beattie [138], P. Becht [97], D. Behera [48], I. Belikov [129], A.D.C. Bell Hechavarria [126], F. Bellini [25], R. Bellwied [116], S. Belokurova [141], L.G.E. Beltran [109], Y.A.V. Beltran [44], G. Bencedi [46], A. Bensaoula[116], S. Beole [24], Y. Berdnikov [141], A. Berdnikova [94], L. Bergmann [94], M.G. Besoiu [63], L. Betev [32], P.P. Bhaduri [135], A. Bhasin [91], B. Bhattacharjee [41], L. Bianchi [24], J. Bielčík [34], J. Bielčíková [86], A.P. Bigot [129], A. Bilandzic [95], G. Biro [46], S. Biswas [4], N. Bize [103], J.T. Blair [108], D. Blau [141], M.B. Blidaru [97], N. Bluhme[38], C. Blume [64], G. Boca [21,55], F. Bock [87], T. Bodova [20], J. Bok [16], L. Boldizsár [46], M. Bombara [36], P.M. Bond [32], G. Bonomi [134,55], H. Borel [130], A. Borissov [141], A.G. Borquez Carcamo [94], E. Botta [24], Y.E.M. Bouziani [64], L. Bratrud [64], P. Braun-Munzinger [97], M. Bregant [110], M. Broz [34], G.E. Bruno [96,31], V.D. Buchakchiev [35], M.D. Buckland [85], D. Budnikov [141], H. Buesching [64], S. Bufalino [29], P. Buhler [102], N. Burmasov [141], Z. Buthelezi [68,123], A. Bylinkin [20], S.A. Bysiak[107], J.C. Cabanillas Noris [109], M.F.T. Cabrera [116], M. Cai [6], H. Caines [138], A. Caliva [28], E. Calvo Villar [101], J.M.M. Camacho [109], P. Camerini [23], F.D.M. Canedo [110], S.L. Cantway [138], M. Carabas [113], A.A. Carballo [32], F. Carnesecchi [32], R. Caron [128], L.A.D. Carvalho [110], J. Castillo Castellanos [130], M. Castoldi [32], F. Catalano [32], S. Cattaruzzi [23], C. Ceballos Sanchez [7], R. Cerri [24], I. Chakaberia [74], P. Chakraborty [136], S. Chandra [135],

S. Chapeland[32], M. Chartier[119], S. Chattopadhay[135], S. Chattopadhyay[135], S. Chattopadhyay[99], M. Chen[39], T. Cheng[6], C. Cheshkov[128], V. Chibante Barroso[32], D.D. Chinellato[102], E.S. Chizzali[II,95], J. Cho[58], S. Cho[58], P. Chochula[32], Z.A. Chochulska[136], D. Choudhury[41], P. Christakoglou[84], C.H. Christensen[83], P. Christiansen[75], T. Chujo[125], M. Ciacco[29], C. Cicalo[52], M.R. Ciupek[97], G. Clai[III,51], F. Colamaria[50], J.S. Colburn[100], D. Colella[31], A. Colelli[31], M. Colocci[25], M. Concas[32], G. Conesa Balbastre[73], Z. Conesa del Valle[131], G. Contin[23], J.G. Contreras[34], M.L. Coquet[103], P. Cortese[133,56], M.R. Cosentino[112], F. Costa[32], S. Costanza[21,55], C. Cot[131], P. Crochet[127], R. Cruz-Torres[74], M.M. Czarnynoga[136], A. Dainese[54], G. Dange[38], M.C. Danisch[94], A. Danu[63], P. Das[80], S. Das[4], A.R. Dash[126], S. Dash[47], A. De Caro[28], G. de Cataldo[50], J. de Cuveland[38], A. De Falco[22], D. De Gruttola[28], N. De Marco[56], C. De Martin[23], S. De Pasquale[28], R. Deb[134], R. Del Grande[95], L. Dello Stritto[32], W. Deng[6], K.C. Devereaux[18], P. Dhankher[18], D. Di Bari[31], A. Di Mauro[32], B. Di Ruzza[132], B. Diab[130], R.A. Diaz[142,7], T. Dietel[114], Y. Ding[6], J. Ditzel[64], R. Divià[32], Ø. Djuvsland[20], U. Dmitrieva[141], A. Dobrin[63], B. Dönigus[64], J.M. Dubinski[136], A. Dubla[97], P. Dupieux[127], N. Dzalaiova[13], T.M. Eder[126], R.J. Ehlers[74], F. Eisenhut[64], R. Ejima[92], D. Elia[50], B. Erazmus[103], F. Ercolessi[25], B. Espagnon[131], G. Eulisse[32], D. Evans[100], S. Evdokimov[141], L. Fabbietti[95], M. Faggin[23], J. Faivre[73], F. Fan[6], W. Fan[74], A. Fantoni[49], M. Fasel[87], A. Feliciello[56], G. Feofilov[141], A. Fernández Téllez[44], L. Ferrandi[110], M.B. Ferrer[32], A. Ferrero[130], C. Ferrero[IV,56], A. Ferretti[24], V.J.G. Feuillard[94], V. Filova[34], D. Finogeev[141], F.M. Fionda[52], E. Flatland[32], F. Flor[138,116], A.N. Flores[108], S. Foertsch[68], I. Fokin[94], S. Fokin[141], U. Follo[IV,56], E. Fragiacomo[57], E. Frajna[46], U. Fuchs[32], N. Funicello[28], C. Furget[73], A. Furs[141], T. Fusayasu[98], J.J. Gaardhøje[83], M. Gagliardi[24], A.M. Gago[101], T. Gahlaut[47], C.D. Galvan[109], S. Gami[80], D.R. Gangadharan[116], P. Ganoti[78], C. Garabatos[97], J.M. Garcia[44], T. García Chávez[44], E. Garcia-Solis[9], C. Gargiulo[32], P. Gasik[97], H.M. Gaur[38], A. Gautam[118], M.B. Gay Ducati[66], M. Germain[103], R.A. Gernhaeuser[95], C. Ghosh[135], M. Giacalone[51], G. Gioachin[29], S.K. Giri[135], P. Giubellino[97,56], P. Giubilato[27], A.M.C. Glaenzer[130], P. Glässel[94], E. Glimos[122], D.J.Q. Goh[76], V. Gonzalez[137], P. Gordeev[141], M. Gorgon[2], K. Goswami[48], S. Gotovac[33], V. Grabski[67], L.K. Graczykowski[136], E. Grecka[86], A. Grelli[59], C. Grigoras[32], V. Grigoriev[141], S. Grigoryan[142,1], F. Grosa[32], J.F. Grosse-Oetringhaus[32], R. Grosso[97], D. Grund[34], N.A. Grunwald[94], G.G. Guardiano[111], R. Guernane[73], M. Guilbaud[103], K. Gulbrandsen[83], J.K. Gumprecht[102], T. Gündem[64], T. Gunji[124], W. Guo[6], A. Gupta[91], R. Gupta[91], R. Gupta[48], K. Gwizdziel[136], L. Gyulai[46], C. Hadjidakis[131], F.U. Haider[91], S. Haidlova[34], M. Haldar[4], H. Hamagaki[76], Y. Han[139], B.G. Hanley[137], R. Hannigan[108], J. Hansen[75], M.R. Haque[97], J.W. Harris[138], A. Harton[9], M.V. Hartung[64], H. Hassan[117], D. Hatzifotiadou[51], P. Hauer[42], L.B. Havener[138], E. Hellbär[32], H. Helstrup[37], M. Hemmer[64], T. Herman[34], S.G. Hernandez[116], G. Herrera Corral[8], S. Herrmann[128], K.F. Hetland[37], B. Heybeck[64], H. Hillemanns[32], B. Hippolyte[129], I.P.M. Hobus[84], F.W. Hoffmann[70], B. Hofman[59], G.H. Hong[139], M. Horst[95], A. Horzyk[2], Y. Hou[6], P. Hristov[32], P. Huhn[64], L.M. Huhta[117], T.J. Humanic[88], A. Hutson[116], D. Hutter[38], M.C. Hwang[18], R. Ilkaev[141], M. Inaba[125], G.M. Innocenti[32], M. Ippolitov[141], A. Isakov[84], T. Isidori[118], M.S. Islam[99], S. Iurchenko[141], M. Ivanov[13], M. Ivanov[97], V. Ivanov[141], K.E. Iversen[75], M. Jablonski[2], B. Jacak[18,74], N. Jacazio[25], P.M. Jacobs[74], S. Jadlovska[106], J. Jadlovsky[106], S. Jaelani[82], C. Jahnke[110], M.J. Jakubowska[136], M.A. Janik[136], T. Janson[70], S. Ji[16], S. Jia[10], T. Jiang[10], A.A.P. Jimenez[65], F. Jonas[74], D.M. Jones[119], J.M. Jowett[32,97], J. Jung[64], M. Jung[64], A. Junique[32], A. Jusko[100], J. Kaewjai[105], P. Kalinak[60], A. Kalweit[32], A. Karasu Uysal[72], D. Karatovic[89], N. Karatzenis[100], O. Karavichev[141], T. Karavicheva[141], E. Karpechev[141], M.J. Karwowska[32,136], U. Kebschull[70], R. Keidel[140], M. Keil[32], B. Ketzer[42], J. Keul[64], S.S. Khade[48], A.M. Khan[120], S. Khan[15], A. Khanzadeev[141], Y. Kharlov[141], A. Khatun[118], A. Khuntia[34], Z. Khuranova[64], B. Kileng[37], B. Kim[104], C. Kim[16], D.J. Kim[117], E.J. Kim[69], J. Kim[139], J. Kim[58], J. Kim[32,69], M. Kim[18], S. Kim[17], T. Kim[139], K. Kimura[92], A. Kirkova[35], S. Kirsch[64], I. Kisel[38], S. Kiselev[141], A. Kisiel[136], J.P. Kitowski[2], J.L. Klay[5], J. Klein[32], S. Klein[74], C. Klein-Bösing[126], M. Kleiner[64], T. Klemenz[95], A. Kluge[32], C. Kobdaj[105], R. Kohara[124], T. Kollegger[97], A. Kondratyev[142], N. Kondratyeva[141], J. Konig[64], S.A. Konigstorfer[95], P.J. Konopka[32], G. Kornakov[136], M. Korwieser[95], S.D. Koryciak[2], C. Koster[84], A. Kotliarov[86], N. Kovacic[89], V. Kovalenko[141], M. Kowalski[107], V. Kozhuharov[35], G. Kozlov[38], I. Králik[60], A. Kravčáková[36], L. Krcal[32,38], M. Krivda[100,60], F. Krizek[86], K. Krizkova Gajdosova[32], C. Krug[66], M. Krüger[64], D.M. Krupova[34], E. Kryshen[141], V. Kučera[58], C. Kuhn[129], P.G. Kuijer[84], T. Kumaoka[125], D. Kumar[135], L. Kumar[90], N. Kumar[90], S. Kumar[50], S. Kundu[32], P. Kurashvili[79], A. Kurepin[141], A.B. Kurepin[141], A. Kuryakin[141], S. Kushpil[86], V. Kuskov[141], M. Kutyla[136], A. Kuznetsov[142], M.J. Kweon[58], Y. Kwon[139], S.L. La Pointe[38], P. La Rocca[26], A. Lakrathok[105], M. Lamanna[32], A.R. Landou[73], R. Langoy[121], P. Larionov[32], E. Laudi[32], L. Lautner[32,95], R.A.N. Laveaga[109], R. Lavicka[102], R. Lea[134,55], H. Lee[104], I. Legrand[45], G. Legras[126], J. Lehrbach[38], A.M. Lejeune[34], T.M. Lelek[2], R.C. Lemmon[I,85], I. León Monzón[109], M.M. Lesch[95], E.D. Lesser[18], P. Lévai[46], M. Li[6], P. Li[10], X. Li[10], B.E. Liang-Gilman[18], J. Lien[121], R. Lietava[100], I. Likmeta[116], B. Lim[24], S.H. Lim[16], V. Lindenstruth[38], C. Lippmann[97], D.H. Liu[6], J. Liu[119], G.S.S. Liveraro[111], I.M. Lofnes[20], C. Loizides[87], S. Lokos[107], J. Lömker[59], X. Lopez[127], E. López Torres[7], C. Lotteau[128], P. Lu[97,120], Z. Lu[10], F.V. Lugo[67], J.R. Luhder[126], M. Lunardon[27], G. Luparello[57], Y.G. Ma[39], M. Mager[32], A. Maire[129], E.M. Majerz[2], M.V. Makariev[35], M. Malaev[141], G. Malfattore[25], N.M. Malik[91], S.K. Malik[91], L. Malinina[I,VIII,142], D. Mallick[131], N. Mallick[48], G. Mandaglio[30,53], S.K. Mandal[79], A. Manea[63], V. Manko[141], F. Manso[127], V. Manzari[50], Y. Mao[6], R.W. Marcjan[2], G.V. Margagliotti[23], A. Margotti[51], A. Marín[97], C. Markert[108], C.F.B. Marquez[31], P. Martinengo[32], M.I. Martínez[44], G. Martínez García[103], M.P.P. Martins[110], S. Masciocchi[97], M. Masera[24], A. Masoni[52], L. Massacrier[131], O. Massen[59], A. Mastroserio[132,50], O. Matonoha[75], S. Mattiazzo[27], A. Matyja[107], F. Mazzaschi[32,24], M. Mazzilli[116], Y. Melikyan[43], M. Melo[110], A. Menchaca-Rocha[67], J.E.M. Mendez[65], E. Meninno[102], A.S. Menon[116], M.W. Menzel[32,94], M. Meres[13], Y. Miake[125], L. Micheletti[32], D.L. Mihaylov[95], A.U. Mikalsen[20], K. Mikhaylov[142,141], N. Minafra[118], D. Miśkowiec[97], A. Modak[134], B. Mohanty[80], M. Mohisin Khan[V,15], M.A. Molander[43], S. Monira[136], C. Mordasini[117], D.A. Moreira De Godoy[126], I. Morozov[141], A. Morsch[32], T. Mrnjavac[32], V. Muccifora[49], S. Muhuri[135], J.D. Mulligan[74], A. Mulliri[22], M.G. Munhoz[110], R.H. Munzer[64], H. Murakami[124], S. Murray[114], L. Musa[32], J. Musinsky[60], J.W. Myrcha[136], B. Naik[123], A.I. Nambrath[18], B.K. Nandi[47], R. Nania[51], E. Nappi[50], A.F. Nassirpour[17], A. Nath[94], S. Nath[135], C. Nattrass[122], M.N. Naydenov[35], A. Neagu[19], A. Negru[113], E. Nekrasova[141], L. Nellen[65], R. Nepeivoda[75], S. Nese[19], N. Nicassio[31], B.S. Nielsen[83], E.G. Nielsen[83], S. Nikolaev[141], S. Nikulin[141], V. Nikulin[141], F. Noferini[51], S. Noh[12], P. Nomokonov[142], J. Norman[119], N. Novitzky[87], P. Nowakowski[136], A. Nyanin[141], J. Nystrand[20], M. Ogino[76], S. Oh[17], A. Ohlson[75], V.A. Okorokov[141], J. Oleniacz[136], A. Onnerstad[117], C. Oppedisano[56], A. Ortiz Velasquez[65], J. Otwinowski[107], M. Oya[92], K. Oyama[76], Y. Pachmayer[94], S. Padhan[47], D. Pagano[134,55], G. Paić[65], S. Paisano-Guzmán[44],

A. Palasciano[50], I. Panasenko[75], S. Panebianco[130], C. Pantouvakis[27], H. Park[125], H. Park[104], J. Park[125], J.E. Parkkila[32], Y. Patley[47], R.N. Patra[50], B. Paul[135], H. Pei[6], T. Peitzmann[59], X. Peng[11], M. Pennisi[24], S. Perciballi[24], D. Peresunko[141], G.M. Perez[7], Y. Pestov[141], M.T. Petersen[83], V. Petrov[141], M. Petrovici[45], S. Piano[57], M. Pikna[13], P. Pillot[103], O. Pinazza[51,32], L. Pinsky[116], C. Pinto[95], S. Pisano[49], M. Płoskoń[74], M. Planinic[89], F. Pliquett[64], D.K. Plociennik[2], M.G. Poghosyan[87], B. Polichtchouk[141], S. Politano[29], N. Poljak[89], A. Pop[45], S. Porteboeuf-Houssais[127], V. Pozdniakov[I,142], I.Y. Pozos[44], K.K. Pradhan[48], S.K. Prasad[4], S. Prasad[48], R. Preghenella[51], F. Prino[56], C.A. Pruneau[137], I. Pshenichnov[141], M. Puccio[32], S. Pucillo[24], S. Qiu[84], L. Quaglia[24], A.M.K. Radhakrishnan[48], S. Ragoni[14], A. Rai[138], A. Rakotozafindrabe[130], L. Ramello[133,56], F. Rami[129], C.O. Ramirez-Alvarez[44], M. Rasa[26], S.S. Räsänen[43], R. Rath[51], M.P. Rauch[20], I. Ravasenga[32], K.F. Read[87,122], C. Reckziegel[112], A.R. Redelbach[38], K. Redlich[VI,79], C.A. Reetz[97], H.D. Regules-Medel[44], A. Rehman[20], F. Reidt[32], H.A. Reme-Ness[37], K. Reygers[94], A. Riabov[141], V. Riabov[141], R. Ricci[28], M. Richter[20], A.A. Riedel[95], W. Riegler[32], A.G. Riffero[24], M. Rignanese[27], C. Ripoli[28], C. Ristea[63], M.V. Rodriguez[32], M. Rodríguez Cahuantzi[44], S.A. Rodríguez Ramírez[44], K. Røed[19], R. Rogalev[141], E. Rogochaya[142], T.S. Rogoschinski[64], D. Rohr[32], D. Röhrich[20], S. Rojas Torres[34], P.S. Rokita[136], G. Romanenko[25], F. Ronchetti[32], E.D. Rosas[65], K. Roslon[136], A. Rossi[54], A. Roy[48], S. Roy[47], N. Rubini[51,25], J.A. Rudolph[84], D. Ruggiano[136], R. Rui[23], P.G. Russek[2], R. Russo[84], A. Rustamov[81], E. Ryabinkin[141], Y. Ryabov[141], A. Rybicki[107], J. Ryu[16], W. Rzesa[136], B. Sabiu[51], S. Sadovsky[141], J. Saetre[20], K. Šafařík[I,34], S. Saha[80], B. Sahoo[48], R. Sahoo[48], S. Sahoo[61], D. Sahu[48], P.K. Sahu[61], J. Saini[135], K. Sajdakova[36], S. Sakai[125], M.P. Salvan[97], S. Sambyal[91], D. Samitz[102], I. Sanna[32,95], T.B. Saramela[110], D. Sarkar[83], P. Sarma[41], V. Sarritzu[22], V.M. Sarti[95], M.H.P. Sas[32], S. Sawan[80], E. Scapparone[51], J. Schambach[87], H.S. Scheid[64], C. Schiaua[45], R. Schicker[94], F. Schlepper[94], A. Schmah[97], C. Schmidt[97], H.R. Schmidt[93], M.O. Schmidt[32], M. Schmidt[93], N.V. Schmidt[87], A.R. Schmier[122], R. Schotter[102,129], A. Schröter[38], J. Schukraft[32], K. Schweda[97], G. Scioli[25], E. Scomparin[56], J.E. Seger[14], Y. Sekiguchi[124], D. Sekihata[124], M. Selina[84], I. Selyuzhenkov[97], S. Senyukov[129], J.J. Seo[94], D. Serebryakov[141], L. Serkin[VII,65], L. Šerkšnytė[95], A. Sevcenco[63], T.J. Shaba[68], A. Shabetai[103], R. Shahoyan[32], A. Shangaraev[141], B. Sharma[91], D. Sharma[47], H. Sharma[54], M. Sharma[91], S. Sharma[76], S. Sharma[91], U. Sharma[91], A. Shatat[131], O. Sheibani[116], K. Shigaki[92], M. Shimomura[77], J. Shin[12], S. Shirinkin[141], Q. Shou[39], Y. Sibiriak[141], S. Siddhanta[52], T. Siemiarczuk[79], T.F. Silva[110], D. Silvermyr[75], T. Simantathammakul[105], R. Simeonov[35], B. Singh[91], B. Singh[95], K. Singh[48], R. Singh[80], R. Singh[91], R. Singh[97], S. Singh[15], V.K. Singh[135], V. Singhal[135], T. Sinha[99], B. Sitar[13], M. Sitta[133,56], T.B. Skaali[19], G. Skorodumovs[94], N. Smirnov[138], R.J.M. Snellings[59], E.H. Solheim[19], J. Song[16], C. Sonnabend[32,97], J.M. Sonneveld[84], F. Soramel[27], A.B. Soto-Hernandez[88], R. Spijkers[84], I. Sputowska[107], J. Staa[75], J. Stachel[94], I. Stan[63], P.J. Steffanic[122], T. Stellhorn[126], S.F. Stiefelmaier[94], D. Stocco[103], I. Storehaug[19], N.J. Strangmann[64], P. Stratmann[126], S. Strazzi[25], A. Sturniolo[30,53], C.P. Stylianidis[84], A.A.P. Suaide[110], C. Suire[131], M. Sukhanov[141], M. Suljic[32], R. Sultanov[141], V. Sumberia[91], S. Sumowidagdo[82], M. Szymkowski[136], L.H. Tabares[7], S.F. Taghavi[95], G. Taillepied[97], J. Takahashi[111], G.J. Tambave[80], S. Tang[6], Z. Tang[120], J.D. Tapia Takaki[118], N. Tapus[113], L.A. Tarasovicova[36], M.G. Tarzila[45], G.F. Tassielli[31], A. Tauro[32], A. Tavira García[131], G. Tejeda Muñoz[44], L. Terlizzi[24], C. Terrevoli[50], S. Thakur[4], D. Thomas[108], A. Tikhonov[141], N. Tiltmann[32,126], A.R. Timmins[116], M. Tkacik[106], T. Tkacik[106], A. Toia[64], R. Tokumoto[92], S. Tomassini[25], K. Tomohiro[92], N. Topilskaya[141], M. Toppi[49], V.V. Torres[103], A.G. Torres Ramos[31], A. Trifiró[30,53], T. Triloki[96], A.S. Triolo[32,30,53], S. Tripathy[32], T. Tripathy[47], S. Trogolo[24], V. Trubnikov[3], W.H. Trzaska[117], T.P. Trzcinski[136], C. Tsolanta[19], R. Tu[39], A. Tumkin[141], R. Turrisi[54], T.S. Tveter[19], K. Ullaland[20], B. Ulukutlu[95], S. Upadhyaya[107], A. Uras[128], M. Urioni[134], G.L. Usai[22], M. Vala[36], N. Valle[55], L.V.R. van Doremalen[59], M. van Leeuwen[84], C.A. van Veen[94], R.J.G. van Weelden[84], P. Vande Vyvre[32], D. Varga[46], Z. Varga[46], P. Vargas Torres[65], M. Vasileiou[78], A. Vasiliev[I,141], O. Vázquez Doce[49], O. Vazquez Rueda[116], V. Vechernin[141], E. Vercellin[24], S. Vergara Limón[44], R. Verma[47], L. Vermunt[97], R. Vértesi[46], M. Verweij[59], L. Vickovic[33], Z. Vilakazi[123], O. Villalobos Baillie[100], A. Villani[23], A. Vinogradov[141], T. Virgili[28], M.M.O. Virta[117], A. Vodopyanov[142], B. Volkel[32], M.A. Völkl[94], S.A. Voloshin[137], G. Volpe[31], B. von Haller[32], I. Vorobyev[32], N. Vozniuk[141], J. Vrláková[36], J. Wan[39], C. Wang[39], D. Wang[39], Y. Wang[39], Y. Wang[6], Z. Wang[39], A. Wegrzynek[32], F.T. Weiglhofer[38], S.C. Wenzel[32], J.P. Wessels[126], J. Wiechula[64], J. Wikne[19], G. Wilk[79], J. Wilkinson[97], G.A. Willems[126], B. Windelband[94], M. Winn[130], J.R. Wright[108], W. Wu[39], Y. Wu[120], Z. Xiong[120], R. Xu[6], A. Yadav[42], A.K. Yadav[135], Y. Yamaguchi[92], S. Yang[20], S. Yano[92], E.R. Yeats[18], Z. Yin[6], I.-K. Yoo[16], J.H. Yoon[58], H. Yu[12], S. Yuan[20], A. Yuncu[94], V. Zaccolo[23], C. Zampolli[32], F. Zanone[94], N. Zardoshti[32], A. Zarochentsev[141], P. Závada[62], N. Zaviyalov[141], M. Zhalov[141], B. Zhang[94,6], C. Zhang[130], L. Zhang[39], M. Zhang[127,6], M. Zhang[6], S. Zhang[39], X. Zhang[6], Y. Zhang[120], Z. Zhang[6], M. Zhao[10], V. Zherebchevskii[141], Y. Zhi[10], D. Zhou[6], Y. Zhou[83], J. Zhu[54,6], S. Zhu[120], Y. Zhu[6], S.C. Zugravel[56], N. Zurlo[134,55]

Affiliation Notes

[I] Deceased
[II] Also at: Max-Planck-Institut fur Physik, Munich, Germany
[III] Also at: Italian National Agency for New Technologies, Energy and Sustainable Economic Development (ENEA), Bologna, Italy
[IV] Also at: Dipartimento DET del Politecnico di Torino, Turin, Italy
[V] Also at: Department of Applied Physics, Aligarh Muslim University, Aligarh, India
[VI] Also at: Institute of Theoretical Physics, University of Wroclaw, Poland
[VII] Also at: Facultad de Ciencias, Universidad Nacional Autónoma de México, Mexico City, Mexico
[VIII] Also at: An institution covered by a cooperation agreement with CERN

Collaboration Institutes

[1] A.I. Alikhanyan National Science Laboratory (Yerevan Physics Institute) Foundation, Yerevan, Armenia
[2] AGH University of Krakow, Cracow, Poland
[3] Bogolyubov Institute for Theoretical Physics, National Academy of Sciences of Ukraine, Kiev, Ukraine
[4] Bose Institute, Department of Physics and Centre for Astroparticle Physics and Space Science (CAPSS), Kolkata, India
[5] California Polytechnic State University, San Luis Obispo, California, United States
[6] Central China Normal University, Wuhan, China
[7] Centro de Aplicaciones Tecnológicas y Desarrollo Nuclear (CEADEN), Havana, Cuba
[8] Centro de Investigación y de Estudios Avanzados (CINVESTAV), Mexico City and Mérida, Mexico
[9] Chicago State University, Chicago, Illinois, United States

[10] China Nuclear Data Center, China Institute of Atomic Energy, Beijing, China
[11] China University of Geosciences, Wuhan, China
[12] Chungbuk National University, Cheongju, Republic of Korea
[13] Comenius University Bratislava, Faculty of Mathematics, Physics and Informatics, Bratislava, Slovak Republic
[14] Creighton University, Omaha, Nebraska, United States
[15] Department of Physics, Aligarh Muslim University, Aligarh, India
[16] Department of Physics, Pusan National University, Pusan, Republic of Korea
[17] Department of Physics, Sejong University, Seoul, Republic of Korea
[18] Department of Physics, University of California, Berkeley, California, United States
[19] Department of Physics, University of Oslo, Oslo, Norway
[20] Department of Physics and Technology, University of Bergen, Bergen, Norway
[21] Dipartimento di Fisica, Università di Pavia, Pavia, Italy
[22] Dipartimento di Fisica dell'Università and Sezione INFN, Cagliari, Italy
[23] Dipartimento di Fisica dell'Università and Sezione INFN, Trieste, Italy
[24] Dipartimento di Fisica dell'Università and Sezione INFN, Turin, Italy
[25] Dipartimento di Fisica e Astronomia dell'Università and Sezione INFN, Bologna, Italy
[26] Dipartimento di Fisica e Astronomia dell'Università and Sezione INFN, Catania, Italy
[27] Dipartimento di Fisica e Astronomia dell'Università and Sezione INFN, Padova, Italy
[28] Dipartimento di Fisica 'E.R. Caianiello' dell'Università and Gruppo Collegato INFN, Salerno, Italy
[29] Dipartimento DISAT del Politecnico and Sezione INFN, Turin, Italy
[30] Dipartimento di Scienze MIFT, Università di Messina, Messina, Italy
[31] Dipartimento Interateneo di Fisica 'M. Merlin' and Sezione INFN, Bari, Italy
[32] European Organization for Nuclear Research (CERN), Geneva, Switzerland
[33] Faculty of Electrical Engineering, Mechanical Engineering and Naval Architecture, University of Split, Split, Croatia
[34] Faculty of Nuclear Sciences and Physical Engineering, Czech Technical University in Prague, Prague, Czech Republic
[35] Faculty of Physics, Sofia University, Sofia, Bulgaria
[36] Faculty of Science, P.J. Šafárik University, Košice, Slovak Republic
[37] Faculty of Technology, Environmental and Social Sciences, Bergen, Norway
[38] Frankfurt Institute for Advanced Studies, Johann Wolfgang Goethe-Universität Frankfurt, Frankfurt, Germany
[39] Fudan University, Shanghai, China
[40] Gangneung-Wonju National University, Gangneung, Republic of Korea
[41] Gauhati University, Department of Physics, Guwahati, India
[42] Helmholtz-Institut für Strahlen- und Kernphysik, Rheinische Friedrich-Wilhelms-Universität Bonn, Bonn, Germany
[43] Helsinki Institute of Physics (HIP), Helsinki, Finland
[44] High Energy Physics Group, Universidad Autónoma de Puebla, Puebla, Mexico
[45] Horia Hulubei National Institute of Physics and Nuclear Engineering, Bucharest, Romania
[46] HUN-REN Wigner Research Centre for Physics, Budapest, Hungary
[47] Indian Institute of Technology Bombay (IIT), Mumbai, India
[48] Indian Institute of Technology Indore, Indore, India
[49] INFN, Laboratori Nazionali di Frascati, Frascati, Italy
[50] INFN, Sezione di Bari, Bari, Italy
[51] INFN, Sezione di Bologna, Bologna, Italy
[52] INFN, Sezione di Cagliari, Cagliari, Italy
[53] INFN, Sezione di Catania, Catania, Italy
[54] INFN, Sezione di Padova, Padova, Italy
[55] INFN, Sezione di Pavia, Pavia, Italy
[56] INFN, Sezione di Torino, Turin, Italy
[57] INFN, Sezione di Trieste, Trieste, Italy
[58] Inha University, Incheon, Republic of Korea
[59] Institute for Gravitational and Subatomic Physics (GRASP), Utrecht University/Nikhef, Utrecht, Netherlands
[60] Institute of Experimental Physics, Slovak Academy of Sciences, Košice, Slovak Republic
[61] Institute of Physics, Homi Bhabha National Institute, Bhubaneswar, India
[62] Institute of Physics of the Czech Academy of Sciences, Prague, Czech Republic
[63] Institute of Space Science (ISS), Bucharest, Romania
[64] Institut für Kernphysik, Johann Wolfgang Goethe-Universität Frankfurt, Frankfurt, Germany
[65] Instituto de Ciencias Nucleares, Universidad Nacional Autónoma de México, Mexico City, Mexico
[66] Instituto de Física, Universidade Federal do Rio Grande do Sul (UFRGS), Porto Alegre, Brazil
[67] Instituto de Física, Universidad Nacional Autónoma de México, Mexico City, Mexico
[68] iThemba LABS, National Research Foundation, Somerset West, South Africa
[69] Jeonbuk National University, Jeonju, Republic of Korea
[70] Johann-Wolfgang-Goethe Universität Frankfurt Institut für Informatik, Fachbereich Informatik und Mathematik, Frankfurt, Germany
[71] Korea Institute of Science and Technology Information, Daejeon, Republic of Korea
[72] KTO Karatay University, Konya, Turkey
[73] Laboratoire de Physique Subatomique et de Cosmologie, Université Grenoble-Alpes, CNRS-IN2P3, Grenoble, France
[74] Lawrence Berkeley National Laboratory, Berkeley, California, United States
[75] Lund University Department of Physics, Division of Particle Physics, Lund, Sweden
[76] Nagasaki Institute of Applied Science, Nagasaki, Japan
[77] Nara Women's University (NWU), Nara, Japan
[78] National and Kapodistrian University of Athens, School of Science, Department of Physics , Athens, Greece
[79] National Centre for Nuclear Research, Warsaw, Poland
[80] National Institute of Science Education and Research, Homi Bhabha National Institute, Jatni, India
[81] National Nuclear Research Center, Baku, Azerbaijan
[82] National Research and Innovation Agency - BRIN, Jakarta, Indonesia
[83] Niels Bohr Institute, University of Copenhagen, Copenhagen, Denmark
[84] Nikhef, National institute for subatomic physics, Amsterdam, Netherlands
[85] Nuclear Physics Group, STFC Daresbury Laboratory, Daresbury, United Kingdom
[86] Nuclear Physics Institute of the Czech Academy of Sciences, Husinec-Řež, Czech Republic
[87] Oak Ridge National Laboratory, Oak Ridge, Tennessee, United States
[88] Ohio State University, Columbus, Ohio, United States
[89] Physics department, Faculty of science, University of Zagreb, Zagreb, Croatia
[90] Physics Department, Panjab University, Chandigarh, India
[91] Physics Department, University of Jammu, Jammu, India
[92] Physics Program and International Institute for Sustainability with Knotted Chiral Meta Matter (WPI-SKCM^2), Hiroshima University, Hiroshima, Japan
[93] Physikalisches Institut, Eberhard-Karls-Universität Tübingen, Tübingen, Germany
[94] Physikalisches Institut, Ruprecht-Karls-Universität Heidelberg, Heidelberg, Germany
[95] Physik Department, Technische Universität München, Munich,

Germany
[96] Politecnico di Bari and Sezione INFN, Bari, Italy
[97] Research Division and ExtreMe Matter Institute EMMI, GSI Helmholtzzentrum für Schwerionenforschung GmbH, Darmstadt, Germany
[98] Saga University, Saga, Japan
[99] Saha Institute of Nuclear Physics, Homi Bhabha National Institute, Kolkata, India
[100] School of Physics and Astronomy, University of Birmingham, Birmingham, United Kingdom
[101] Sección Física, Departamento de Ciencias, Pontificia Universidad Católica del Perú, Lima, Peru
[102] Stefan Meyer Institut für Subatomare Physik (SMI), Vienna, Austria
[103] SUBATECH, IMT Atlantique, Nantes Université, CNRS-IN2P3, Nantes, France
[104] Sungkyunkwan University, Suwon City, Republic of Korea
[105] Suranaree University of Technology, Nakhon Ratchasima, Thailand
[106] Technical University of Košice, Košice, Slovak Republic
[107] The Henryk Niewodniczanski Institute of Nuclear Physics, Polish Academy of Sciences, Cracow, Poland
[108] The University of Texas at Austin, Austin, Texas, United States
[109] Universidad Autónoma de Sinaloa, Culiacán, Mexico
[110] Universidade de São Paulo (USP), São Paulo, Brazil
[111] Universidade Estadual de Campinas (UNICAMP), Campinas, Brazil
[112] Universidade Federal do ABC, Santo Andre, Brazil
[113] Universitatea Nationala de Stiinta si Tehnologie Politehnica Bucuresti, Bucharest, Romania
[114] University of Cape Town, Cape Town, South Africa
[115] University of Derby, Derby, United Kingdom
[116] University of Houston, Houston, Texas, United States
[117] University of Jyväskylä, Jyväskylä, Finland
[118] University of Kansas, Lawrence, Kansas, United States
[119] University of Liverpool, Liverpool, United Kingdom
[120] University of Science and Technology of China, Hefei, China
[121] University of South-Eastern Norway, Kongsberg, Norway
[122] University of Tennessee, Knoxville, Tennessee, United States
[123] University of the Witwatersrand, Johannesburg, South Africa
[124] University of Tokyo, Tokyo, Japan
[125] University of Tsukuba, Tsukuba, Japan
[126] Universität Münster, Institut für Kernphysik, Münster, Germany
[127] Université Clermont Auvergne, CNRS/IN2P3, LPC, Clermont-Ferrand, France
[128] Université de Lyon, CNRS/IN2P3, Institut de Physique des 2 Infinis de Lyon, Lyon, France
[129] Université de Strasbourg, CNRS, IPHC UMR 7178, F-67000 Strasbourg, France, Strasbourg, France
[130] Université Paris-Saclay, Centre d'Etudes de Saclay (CEA), IRFU, Départment de Physique Nucléaire (DPhN), Saclay, France
[131] Université Paris-Saclay, CNRS/IN2P3, IJCLab, Orsay, France
[132] Università degli Studi di Foggia, Foggia, Italy
[133] Università del Piemonte Orientale, Vercelli, Italy
[134] Università di Brescia, Brescia, Italy
[135] Variable Energy Cyclotron Centre, Homi Bhabha National Institute, Kolkata, India
[136] Warsaw University of Technology, Warsaw, Poland
[137] Wayne State University, Detroit, Michigan, United States
[138] Yale University, New Haven, Connecticut, United States
[139] Yonsei University, Seoul, Republic of Korea
[140] Zentrum für Technologie und Transfer (ZTT), Worms, Germany
[141] Affiliated with an institute covered by a cooperation agreement with CERN
[142] Affiliated with an international laboratory covered by a cooperation agreement with CERN.

References

[1] Z.-T. Lu, P. Mueller, G.W.F. Drake, W. Noertershaeuser, S.C. Pieper, Z.C. Yan, Colloquium: laser probing of neutron-rich nuclei in light atoms, Rev. Mod. Phys. 85 (4) (2013) 1383–1400. https://doi.org/10.1103/RevModPhys.85.1383

[2] H. Heylen, et al., High-resolution laser spectroscopy of $^{27-32}$Al, Phys. Rev. C 103 (1) (2021) 014318. https://doi.org/10.1103/PhysRevC.103.014318

[3] N. Bree, et al., Shape coexistence in the neutron-deficient even-even $^{182-188}$Hg isotopes studied via coulomb excitation, Phys. Rev. Lett. 112 (16) (2014) 162701. https://doi.org/10.1103/PhysRevLett.112.162701

[4] A.D. Ayangeakaa, et al., Evidence for rigid triaxial deformation in ^{76}Ge from a model-independent analysis, Phys. Rev. Lett. 123 (10) (2019) 102501. arXiv preprint arXiv:1909.03270, https://doi.org/10.1103/PhysRevLett.123.102501

[5] A. Koszorús, et al., Charge radii of exotic potassium isotopes challenge nuclear theory and the magic character of $N = 32$, Nature Phys. 17 (4) (2021) 439–443. [Erratum: Nature Phys. 17, 539 (2021)]. arXiv preprint arXiv:2012.01864, https://doi.org/10.1038/s41567-020-01136-5

[6] J. Warbinek, et al., Smooth trends in fermium charge radii and the impact of shell effects, Nature 634 (8036) (2024) 1075–1079. https://doi.org/10.1038/s41586-024-08062-z

[7] H. Hergert, A guided tour of *ab initio* nuclear many-body theory, Front. Phys. 8 (2020) 379. arXiv preprint arXiv:2008.05061, https://doi.org/10.3389/fphy.2020.00379

[8] S. Gandolfi, D. Lonardoni, A. Lovato, M. Piarulli, Atomic nuclei from quantum Monte Carlo calculations with chiral EFT interactions, Front. Phys. 8 (2020) 117. arXiv preprint arXiv:2001.01374, https://doi.org/10.3389/fphy.2020.00117

[9] V. Somà, Self-consistent Green's function theory for atomic nuclei, Front. Phys. 8 (2020) 340. arXiv preprint arXiv:2003.11321, https://doi.org/10.3389/fphy.2020.00340

[10] T.A. Lähde, U.-G. Meißner, Nuclear Lattice Effective Field Theory: An introduction, 957, Springer, 2019. https://doi.org/10.1007/978-3-030-14189-9

[11] A. Ekström, C. Forssén, G. Hagen, G.R. Jansen, W. Jiang, T. Papenbrock, What is ab initio in nuclear theory?, Front. Phys. 11 (2023) 1129094. arXiv preprint arXiv:2212.11064, https://doi.org/10.3389/fphy.2023.1129094

[12] B. Hu, et al., Ab initio predictions link the neutron skin of ^{208}Pb to nuclear forces, Nature Phys. 18 (10) (2022) 1196–1200. arXiv preprint arXiv:2112.01125, https://doi.org/10.1038/s41567-023-02324-9

[13] T. Miyagi, S.R. Stroberg, P. Navrátil, K. Hebeler, J.D. Holt, Converged ab initio calculations of heavy nuclei, Phys. Rev. C 105 (1) (2022) 014302. arXiv preprint arXiv:2104.04688, https://doi.org/10.1103/PhysRevC.105.014302

[14] L. Adamczyk, et al., STAR, Azimuthal anisotropy in U+U and Au+Au collisions at RHIC, Phys. Rev. Lett. 115 (22) (2015) 222301. arXiv preprint arXiv:1505.07812, https://doi.org/10.1103/PhysRevLett.115.222301

[15] M. Abdallah, et al., STAR, Search for the chiral magnetic effect with isobar collisions at $\sqrt{s_{\rm NN}} = 200$ GeV by the STAR collaboration at the BNL relativistic heavy ion collider, Phys. Rev. C 105 (1) (2022) 014901. arXiv preprint arXiv:2109.00131, https://doi.org/10.1103/PhysRevC.105.014901

[16] C. Zhang, J. Jia, Evidence of quadrupole and octupole deformations in ^{96}Zr+^{96}Zr and ^{96}Ru+^{96}Ru collisions at ultrarelativistic energies, Phys. Rev. Lett. 128 (2) (2022) 022301. arXiv preprint arXiv:2109.01631, https://doi.org/10.1103/PhysRevLett.128.022301

[17] M.I. Abdulhamid, et al., STAR, Imaging shapes of atomic nuclei in high-energy nuclear collisions, Nature 635 (8037) (2024) 67–72. arXiv preprint arXiv:2401.06625, https://doi.org/10.1038/s41586-024-08097-2

[18] X.-L. Zhao, G.-L. Ma, Y. Zhou, Z.-W. Lin, C. Zhang, Nuclear cluster structure effect in ^{16}O + ^{16}O collisions at the top RHIC energy (2024). arXiv preprint arXiv:2404.09780

[19] S. Acharya, et al., ALICE, Anisotropic flow in Xe-Xe collisions at $\sqrt{s_{\rm NN}} = 5.44$ TeV, Phys. Lett. B 784 (2018) 82–95. arXiv preprint arXiv:1805.01832, https://doi.org/10.1016/j.physletb.2018.06.059

[20] S. Acharya, et al., ALICE, Centrality determination using the glauber model in Xe-Xe collisions at $\sqrt{s_{\rm NN}} = 5.44$ TeV (2018). https://cds.cern.ch/record/2315401. arXiv preprint arXiv:ALICE-PUBLIC-2018-003

[21] S. Acharya, et al., ALICE, Centrality and pseudorapidity dependence of the charged-particle multiplicity density in Xe–Xe collisions at $\sqrt{s_{\rm NN}} = 5.44$ TeV, Phys. Lett. B 790 (2019) 35–48. arXiv preprint arXiv:1805.04432, https://doi.org/10.1016/j.physletb.2018.12.048

[22] G. Aad, et al., ATLAS, Correlations between flow and transverse momentum in Xe+Xe and Pb+Pb collisions at the LHC with the ATLAS detector: a probe of the heavy-ion initial state and nuclear deformation, Phys. Rev. C 107 (5) (2023) 054910. arXiv preprint arXiv:2205.00039, https://doi.org/10.1103/PhysRevC.107.054910

[23] A.M. Sirunyan, et al., CMS, Charged-particle angular correlations in XeXe collisions at $\sqrt{s_{\rm NN}} = 5.44$ TeV, Phys. Rev. C 100 (4) (2019) 044902. arXiv preprint arXiv:1901.07997, https://doi.org/10.1103/PhysRevC.100.044902

[24] G. Giacalone, J. Jia, C. Zhang, Impact of nuclear deformation on relativistic heavy-ion collisions: assessing consistency in nuclear physics across energy scales, Phys. Rev. Lett. 127 (24) (2021) 242301. arXiv preprint arXiv:2105.01638, https://doi.org/10.1103/PhysRevLett.127.242301

[25] S. Zhao, H.-j. Xu, Y.-X. Liu, H. Song, Probing the nuclear deformation with three-particle asymmetric cumulant in RHIC isobar runs, Phys. Lett. B 839 (2023) 137838. arXiv preprint arXiv:2204.02387, https://doi.org/10.1016/j.physletb.2023.137838

[26] S. Acharya, et al., ALICE, Characterizing the initial conditions of heavy-ion collisions at the LHC with mean transverse momentum and anisotropic flow cor-

relations, Phys. Lett. B 834 (2022) 137393. arXiv preprint arXiv:2111.06106, https://doi.org/10.1016/j.physletb.2022.137393
[27] B. Bally, M. Bender, G. Giacalone, V. Somà, Evidence of the triaxial structure of ^{129}Xe at the large hadron collider, Phys. Rev. Lett. 128 (8) (2022) 082301. arXiv preprint arXiv:2108.09578, https://doi.org/10.1103/PhysRevLett.128.082301
[28] H.-j. Xu, J. Zhao, F. Wang, Hexadecapole deformation of U238 from relativistic heavy-ion collisions using a nonlinear response coefficient, Phys. Rev. Lett. 132 (26) (2024) 262301. arXiv preprint arXiv:2402.16550, https://doi.org/10.1103/PhysRevLett.132.262301
[29] W. Ryssens, G. Giacalone, B. Schenke, C. Shen, Evidence of hexadecapole deformation in uranium-238 at the relativistic heavy ion collider, Phys. Rev. Lett. 130 (21) (2023) 212302. arXiv preprint arXiv:2302.13617, https://doi.org/10.1103/PhysRevLett.130.212302
[30] G. Giacalone, G. Nijs, W. van der Schee, Determination of the neutron skin of ^{208}pb from ultrarelativistic nuclear collisions, Phys. Rev. Lett. 131 (20) (2023) 202302. arXiv preprint arXiv:2305.00015, https://doi.org/10.1103/PhysRevLett.131.202302
[31] H. Li, H.-j. Xu, Y. Zhou, X. Wang, J. Zhao, L.-W. Chen, F. Wang, Probing the neutron skin with ultrarelativistic isobaric collisions, Phys. Rev. Lett. 125 (22) (2020) 222301. arXiv preprint arXiv:1910.06170, https://doi.org/10.1103/PhysRevLett.125.222301
[32] H.-j. Xu, W. Zhao, H. Li, Y. Zhou, L.-W. Chen, F. Wang, Probing nuclear structure with mean transverse momentum in relativistic isobar collisions, Phys. Rev. C 108 (1) (2023) L011902. arXiv preprint arXiv:2111.14812, https://doi.org/10.1103/PhysRevC.108.L011902
[33] J. Jia, Probing triaxial deformation of atomic nuclei in high-energy heavy ion collisions, Phys. Rev. C 105 (4) (2022) 044905. arXiv preprint arXiv:2109.00604, https://doi.org/10.1103/PhysRevC.105.044905
[34] J. Jia, Shape of atomic nuclei in heavy ion collisions, Phys. Rev. C 105 (1) (2022) 014905. arXiv preprint arXiv:2106.08768, https://doi.org/10.1103/PhysRevC.105.014905
[35] N. Magdy, Impact of nuclear deformation on collective flow observables in relativistic U + U collisions, Eur. Phys. J. A 59 (3) (2023) 64. arXiv preprint arXiv:2206.05332, https://doi.org/10.1140/epja/s10050-023-00982-0
[36] E.G.D. Nielsen, F.K. Rømer, K. Gulbrandsen, Y. Zhou, Generic multi-particle transverse momentum correlations as a new tool for studying nuclear structure at the energy frontier, Eur. Phys. J. A 60 (2) (2024) 38. arXiv preprint arXiv:2312.00492, https://doi.org/10.1140/epja/s10050-024-01266-x
[37] Z. Lu, M. Zhao, X. Li, J. Jia, Y. Zhou, Probe nuclear structure using the anisotropic flow at the large hadron collider, Eur. Phys. J. A 59 (11) (2023) 279. arXiv preprint arXiv:2309.09663, https://doi.org/10.1140/epja/s10050-023-01194-2
[38] S. Zhao, H.-j. Xu, Y. Zhou, Y.-X. Liu, H. Song, Exploring the nuclear shape phase transition in ultra-relativistic ^{129}Xe + ^{129}Xe collisions at the LHC (2024). arXiv preprint arXiv:2403.07441
[39] B. Muller, J. Schukraft, B. Wyslouch, First results from Pb + Pb collisions at the LHC, Ann. Rev. Nucl. Part. Sci. 62 (2012) 361–386. arXiv preprint arXiv:1202.3233, https://doi.org/10.1146/annurev-nucl-102711-094910
[40] H.-J. Drescher, A. Dumitru, C. Gombeaud, J.-Y. Ollitrault, The centrality dependence of elliptic flow, the hydrodynamic limit, and the viscosity of hot QCD, Phys. Rev. C 76 (2007) 024905. arXiv preprint arXiv:0704.3553, https://doi.org/10.1103/PhysRevC.76.024905
[41] U. Heinz, R. Snellings, Collective flow and viscosity in relativistic heavy-ion collisions, Ann. Rev. Nucl. Part. Sci. 63 (2013) 123–151. arXiv preprint arXiv:1301.2826, https://doi.org/10.1146/annurev-nucl-102212-170540
[42] D. Molnar, M. Gyulassy, Saturation of elliptic flow and the transport opacity of the gluon plasma at RHIC, Nucl. Phys. A 697 (2002) 495–520. [Erratum: Nucl.Phys.A 703, 893–894 (2002)]. arXiv preprint arXiv:nucl-th/0104073, https://doi.org/10.1016/S0375-9474(01)01224-6
[43] H. Song, Y. Zhou, K. Gajdosova, Collective flow and hydrodynamics in large and small systems at the LHC, Nucl. Sci. Tech. 28 (7) (2017) 99. arXiv preprint arXiv:1703.00670, https://doi.org/10.1007/s41365-017-0245-4
[44] S. Acharya, et al., ALICE, The ALICE experiment: a journey through QCD, Eur. Phys. J. C 84 (8) (2024) 813. arXiv preprint arXiv:2211.04384, https://doi.org/10.1140/epjc/s10052-024-12935-y
[45] S. Voloshin, Y. Zhang, Flow study in relativistic nuclear collisions by fourier expansion of azimuthal particle distributions, Z. Phys. C 70 (1996) 665–672. arXiv preprint arXiv:hep-ph/9407282, https://doi.org/10.1007/s002880050141
[46] K. Aamodt, et al., ALICE, Higher harmonic anisotropic flow measurements of charged particles in Pb–Pb collisions at $\sqrt{s_{_{NN}}} = 2.76$ TeV, Phys. Rev. Lett. 107 (2011) 032301. arXiv preprint arXiv:1105.3865, https://doi.org/10.1103/PhysRevLett.107.032301
[47] J. Adam, et al., ALICE, Anisotropic flow of charged particles in Pb–Pb collisions at $\sqrt{s_{_{NN}}} = 5.02$ TeV, Phys. Rev. Lett. 116 (13) (2016) 132302. arXiv preprint arXiv:1602.01119, https://doi.org/10.1103/PhysRevLett.116.132302
[48] S. Acharya, et al., ALICE, Investigations of anisotropic flow using multiparticle azimuthal correlations in pp, p–Pb, Xe–Xe, and Pb–Pb collisions at the LHC, Phys. Rev. Lett. 123 (14) (2019) 142301. arXiv preprint arXiv:1903.01790, https://doi.org/10.1103/PhysRevLett.123.142301
[49] G. Aad, et al., ATLAS, Measurement of the azimuthal anisotropy for charged particle production in $\sqrt{s_{_{NN}}} = 2.76$ TeV lead-lead collisions with the ATLAS detector, Phys. Rev. C 86 (2012) 014907. arXiv preprint arXiv:1203.3087, https://doi.org/10.1103/PhysRevC.86.014907
[50] G. Aad, et al., ATLAS, Measurement of the azimuthal anisotropy of charged-particle production in Xe+Xe collisions at $\sqrt{s_{_{NN}}} = 5.44$ TeV with the ATLAS detector, Phys. Rev. C 101 (2) (2020) 024906. arXiv preprint arXiv:1911.04812, https://doi.org/10.1103/PhysRevC.101.024906
[51] S. Chatrchyan, et al., CMS, Measurement of higher-Order harmonic azimuthal anisotropy in PbPb collisions at $\sqrt{s_{_{NN}}} = 2.76$ TeV, Phys. Rev. C 89 (4) (2014) 044906. arXiv preprint arXiv:1310.8651, https://doi.org/10.1103/PhysRevC.89.044906
[52] S. Acharya, et al., ALICE, Energy dependence and fluctuations of anisotropic flow in Pb–Pb collisions at $\sqrt{s_{NN}} = 5.02$ and 2.76 TeV, JHEP 07 (2018) 103. arXiv preprint arXiv:1804.02944, https://doi.org/10.1007/JHEP07(2018)103
[53] S. Acharya, et al., ALICE, Observation of flow angle and flow magnitude fluctuations in Pb-Pb collisions at $\sqrt{s_{_{NN}}}$ =5.02Tev at the CERN large hadron collider, Phys. Rev. C 107 (5) (2023) L051901. arXiv preprint arXiv:2206.04574, https://doi.org/10.1103/PhysRevC.107.L051901
[54] S. Acharya, et al., ALICE, Systematic study of flow vector fluctuations in $\sqrt{s_{_{NN}}}$ =5.02 TeV Pb-Pb collisions, Phys. Rev. C 109 (6) (2024) 065202. arXiv preprint arXiv:2403.15213, https://doi.org/10.1103/PhysRevC.109.065202
[55] S. Acharya, et al., ALICE, Pseudorapidity dependence of anisotropic flow and its decorrelations using long-range multiparticle correlations in Pb–Pb and Xe–Xe collisions, Phys. Lett. B 850 (2024) 138477. [Erratum: Phys.Lett.B 853, 138659 (2024)]. arXiv preprint arXiv:2307.11116, https://doi.org/10.1016/j.physletb.2024.138477
[56] G. Aad, et al., ATLAS, Measurement of the distributions of event-by-event flow harmonics in lead-lead collisions at $\sqrt{s_{_{NN}}} = 2.76$ TeV with the ATLAS detector at the LHC, JHEP 11 (2013) 183. arXiv preprint arXiv:1305.2942, https://doi.org/10.1007/JHEP11(2013)183
[57] A.M. Sirunyan, et al., CMS, Non-Gaussian elliptic-flow fluctuations in PbPb collisions at $\sqrt{s_{_{NN}}} = 5.02$ TeV, Phys. Lett. B 789 (2019) 643–665. arXiv preprint arXiv:1711.05594, https://doi.org/10.1016/j.physletb.2018.11.063
[58] J. Adam, et al., ALICE, Correlated event-by-event fluctuations of flow harmonics in Pb–Pb collisions at $\sqrt{s_{_{NN}}} = 2.76$ TeV, Phys. Rev. Lett. 117 (2016) 182301. arXiv preprint arXiv:1604.07663, https://doi.org/10.1103/PhysRevLett.117.182301
[59] S. Acharya, et al., ALICE, Linear and non-linear flow modes in Pb–Pb collisions at $\sqrt{s_{_{NN}}} = 2.76$ TeV, Phys. Lett. B 773 (2017) 68–80. arXiv preprint arXiv:1705.04377, https://doi.org/10.1016/j.physletb.2017.07.060
[60] S. Acharya, et al., ALICE, Systematic studies of correlations between different order flow harmonics in Pb–Pb collisions at $\sqrt{s_{_{NN}}} = 2.76$ TeV, Phys. Rev. C 97 (2) (2018) 024906. arXiv preprint arXiv:1709.01127, https://doi.org/10.1103/PhysRevC.97.024906
[61] S. Acharya, et al., ALICE, Higher harmonic non-linear flow modes of charged hadrons in Pb-Pb collisions at $\sqrt{s_{NN}} = 5.02$ TeV, JHEP 05 (2020) 085. arXiv preprint arXiv:2002.00633, https://doi.org/10.1007/JHEP05(2020)085
[62] S. Acharya, et al., ALICE, Measurements of mixed harmonic cumulants in Pb–Pb collisions at $\sqrt{s_{_{NN}}} = 5.02$ TeV, Phys. Lett. B 818 (2021) 136354. arXiv preprint arXiv:2102.12180, https://doi.org/10.1016/j.physletb.2021.136354
[63] G. Aad, et al., ATLAS, Measurement of the correlation between flow harmonics of different order in lead-lead collisions at $\sqrt{s_{_{NN}}} = 2.76$ TeV with the ATLAS detector, Phys. Rev. C 92 (3) (2015) 034903. arXiv preprint arXiv:1504.01289, https://doi.org/10.1103/PhysRevC.92.034903
[64] J.E. Parkkila, A. Onnerstad, D.J. Kim, Bayesian estimation of the specific shear and bulk viscosity of the quark-gluon plasma with additional flow harmonic observables, Phys. Rev. C 104 (5) (2021) 054904. arXiv preprint arXiv:2106.05019, https://doi.org/10.1103/PhysRevC.104.054904
[65] H. Niemi, G.S. Denicol, H. Holopainen, P. Huovinen, Event-by-event distributions of azimuthal asymmetries in ultrarelativistic heavy-ion collisions, Phys. Rev. C 87 (5) (2013) 054901. arXiv preprint arXiv:1212.1008, https://doi.org/10.1103/PhysRevC.87.054901
[66] H. Song, S.A. Bass, U. Heinz, T. Hirano, C. Shen, 200 A GeV Au + Au collisions serve a nearly perfect quark-gluon liquid, Phys. Rev. Lett. 106 (2011) 192301. [Erratum: Phys.Rev.Lett. 109, 139904 (2012)]. arXiv preprint arXiv:1011.2783, https://doi.org/10.1103/PhysRevLett.106.192301
[67] A. Bilandzic, C.H. Christensen, K. Gulbrandsen, A. Hansen, Y. Zhou, Generic framework for anisotropic flow analyses with multiparticle azimuthal correlations, Phys. Rev. C 89 (6) (2014) 064904. arXiv preprint arXiv:1312.3572, https://doi.org/10.1103/PhysRevC.89.064904
[68] X. Zhu, Y. Zhou, H. Xu, H. Song, Correlations of flow harmonics in 2.76a TeV Pb–Pb collisions, Phys. Rev. C 95 (4) (2017) 044902. arXiv preprint arXiv:1608.05305, https://doi.org/10.1103/PhysRevC.95.044902
[69] K. Hagino, N.W. Lwin, M. Yamagami, Deformation parameter for diffuse density, Phys. Rev. C 74 (2006) 017310. arXiv preprint arXiv:nucl-th/0604048, https://doi.org/10.1103/PhysRevC.74.017310
[70] S. Raman, C.W.G. Nestor, Jr, P. Tikkanen, Transition probability from the ground to the first-excited 2^+ state of even-even nuclides, Atom. Data Nucl. Data Tabl. 78 (2001) 1–128. https://doi.org/10.1006/adnd.2001.0858
[71] B. Pritychenko, M. Birch, B. Singh, M. Horoi, Tables of E2 transition probabilities from the first 2^+ states in even-even nuclei, Atom. Data Nucl. Data Tabl. 107 (2016) 1–139. [Erratum: Atom.Data Nucl.Data Tabl. 114, 371–374 (2017)]. arXiv preprint arXiv:1312.5975, https://doi.org/10.1016/j.adt.2015.10.001
[72] J. Henderson, Convergence of electric quadrupole rotational invariants from the nuclear shell model, Phys. Rev. C 102 (5) (2020) 054306. arXiv preprint arXiv:2005.11210, https://doi.org/10.1103/PhysRevC.102.054306
[73] J. Jia, et al., Imaging the initial condition of heavy-ion collisions and nuclear structure across the nuclide chart, Nucl. Sci. Tech. 35 (12) (2024) 220. arXiv preprint arXiv:2209.11042, https://doi.org/10.1007/s41365-024-01589-w
[74] A. Bilandzic, R. Snellings, S. Voloshin, Flow analysis with cumulants: direct calculations, Phys. Rev. C 83 (2011) 044913. arXiv preprint arXiv:1010.0233, https://doi.org/10.1103/PhysRevC.83.044913

[75] N. Borghini, P.M. Dinh, J.-Y. Ollitrault, A new method for measuring azimuthal distributions in nucleus-nucleus collisions, Phys. Rev. C 63 (2001) 054906. arXiv preprint arXiv:nucl-th/0007063, https://doi.org/10.1103/PhysRevC.63.054906
[76] Z. Moravcova, K. Gulbrandsen, Y. Zhou, Generic algorithm for multiparticle cumulants of azimuthal correlations in high energy nucleus collisions, Phys. Rev. C 103 (2) (2021) 024913. arXiv preprint arXiv:2005.07974, https://doi.org/10.1103/PhysRevC.103.024913
[77] S.A. Voloshin, A.M. Poskanzer, A. Tang, G. Wang, Elliptic flow in the gaussian model of eccentricity fluctuations, Phys. Lett. B 659 (2008) 537–541. arXiv preprint arXiv:0708.0800, https://doi.org/10.1016/j.physletb.2007.11.043
[78] B. Alver, G. Roland, Collision geometry fluctuations and triangular flow in heavy-ion collisions, Phys. Rev. C 81 (2010) 054905. [Erratum: Phys.Rev.C 82, 039903 (2010)]. arXiv preprint arXiv:1003.0194, https://doi.org/10.1103/PhysRevC.82.039903
[79] R.S. Bhalerao, J.-Y. Ollitrault, S. Pal, Characterizing flow fluctuations with moments, Phys. Lett. B 742 (2015) 94–98. arXiv preprint arXiv:1411.5160, https://doi.org/10.1016/j.physletb.2015.01.019
[80] R.S. Bhalerao, J.-Y. Ollitrault, S. Pal, Event-plane correlators, Phys. Rev. C 88 (2013) 024909. arXiv preprint arXiv:1307.0980, https://doi.org/10.1103/PhysRevC.88.024909
[81] L. Yan, J.-Y. Ollitrault, v_4, v_5, v_6, v_7: Nonlinear hydrodynamic response versus LHC data, Phys. Lett. B 744 (2015) 82–87. arXiv preprint arXiv:1502.02502, https://doi.org/10.1016/j.physletb.2015.03.040
[82] Y. Zhou, K. Xiao, Z. Feng, F. Liu, R. Snellings, Anisotropic distributions in a multiphase transport model, Phys. Rev. C 93 (3) (2016) 034909. arXiv preprint arXiv:1508.03306, https://doi.org/10.1103/PhysRevC.93.034909
[83] J. Qian, U.W. Heinz, J. Liu, Mode-coupling effects in anisotropic flow in heavy-ion collisions, Phys. Rev. C 93 (6) (2016) 064901. arXiv preprint arXiv:1602.02813, https://doi.org/10.1103/PhysRevC.93.064901
[84] J.E. Parkkila, A. Onnerstad, S.F. Taghavi, C. Mordasini, A. Bilandzic, M. Virta, D.J. Kim, New constraints for QCD matter from improved bayesian parameter estimation in heavy-ion collisions at LHC, Phys. Lett. B 835 (2022) 137485. arXiv preprint arXiv:2111.08145, https://doi.org/10.1016/j.physletb.2022.137485
[85] P. Huo, K. Gajdošová, J. Jia, Y. Zhou, Importance of non-flow in mixed-harmonic multi-particle correlations in small collision systems, Phys. Lett. B 777 (2018) 201–206. arXiv preprint arXiv:1710.07567, https://doi.org/10.1016/j.physletb.2017.12.035
[86] B.B. Abelev, et al., ALICE, Multiparticle azimuthal correlations in p–Pb and Pb–Pb collisions at the CERN large hadron collider, Phys. Rev. C 90 (5) (2014) 054901. arXiv preprint arXiv:1406.2474, https://doi.org/10.1103/PhysRevC.90.054901
[87] K. Aamodt, et al., ALICE, The ALICE experiment at the CERN LHC, JINST 3 (2008) S08002. https://doi.org/10.1088/1748-0221/3/08/S08002
[88] P. Cortese, et al., ALICE, ALICE: Physics performance report, volume i, J. Phys. G 30 (2004) 1517–1763. https://doi.org/10.1088/0954-3899/30/11/001
[89] C.W. Fabjan, et al., ALICE, ALICE: Physics performance report, volume II, J. Phys. G 32 (2006) 1295–2040. https://doi.org/10.1088/0954-3899/32/10/001
[90] B.B. Abelev, et al., ALICE, Performance of the ALICE experiment at the CERN LHC, Int. J. Mod. Phys. A 29 (2014) 1430044. arXiv preprint arXiv:1402.4476, https://doi.org/10.1142/S0217751X14300440
[91] E. Abbas, et al., ALICE, Performance of the ALICE VZERO system, JINST 8 (2013) P10016. arXiv preprint arXiv:1306.3130, https://doi.org/10.1088/1748-0221/8/10/P10016
[92] K. Aamodt, et al., ALICE, Alignment of the ALICE inner tracking system with cosmic-ray tracks, JINST 5 (2010) P03003. arXiv preprint arXiv:1001.0502, https://doi.org/10.1088/1748-0221/5/03/P03003
[93] J. Alme, et al., The ALICE TPC, a large 3-dimensional tracking device with fast readout for ultra-high multiplicity events, Nucl. Instrum. Meth. A 622 (2010) 316–367. arXiv preprint arXiv:1001.1950, https://doi.org/10.1016/j.nima.2010.04.042
[94] B. Abelev, et al., ALICE, Centrality determination of Pb–Pb collisions at $\sqrt{s_{\rm NN}} = 2.76$ TeV with ALICE, Phys. Rev. C 88 (4) (2013) 044909. arXiv preprint arXiv:1301.4361, https://doi.org/10.1103/PhysRevC.88.044909
[95] X.-N. Wang, M. Gyulassy, HIJING: A Monte Carlo model for multiple jet production in p p, p A and A A collisions, Phys. Rev. D 44 (1991) 3501–3516. https://doi.org/10.1103/PhysRevD.44.3501
[96] M. Gyulassy, X.-N. Wang, HIJING 1.0: A Monte Carlo program for parton and particle production in high-energy hadronic and nuclear collisions, Comput. Phys. Commun. 83 (1994) 307. arXiv preprint arXiv:nucl-th/9502021, https://doi.org/10.1016/0010-4655(94)90057-4
[97] R. Brun, et al., GEANT: Detector Description and Simulation Tool, CERN Program Library, CERN, Geneva, 1993. Long Writeup W5013, https://doi.org/10.17181/CERN.MUHF.DMJ1
[98] R. Barlow, Systematic errors: facts and fictions, in: Conference on Advanced Statistical Techniques in Particle Physics, 2002, pp. 134–144. arXiv preprint arXiv:hep-ex/0207026
[99] B. Schenke, C. Shen, P. Tribedy, Running the gamut of high energy nuclear collisions, Phys. Rev. C 102 (4) (2020) 044905. arXiv preprint arXiv:2005.14682, https://doi.org/10.1103/PhysRevC.102.044905
[100] H. Mäntysaari, B. Schenke, C. Shen, W. Zhao, Bayesian inference of the fluctuating proton shape, Phys. Lett. B 833 (2022) 137348. arXiv preprint arXiv:2202.01998, https://doi.org/10.1016/j.physletb.2022.137348
[101] Q. Liu, S. Zhao, H.-j. Xu, H. Song, Determining the neutron skin thickness by relativistic semi-isobaric collisions, Phys. Rev. C 109 (3) (2024) 034912. arXiv preprint arXiv:2311.01747, https://doi.org/10.1103/PhysRevC.109.034912
[102] M. Abdallah, et al., STAR, Collision-system and beam-energy dependence of anisotropic flow fluctuations, Phys. Rev. Lett. 129 (25) (2022) 252301. arXiv preprint arXiv:2201.10365, https://doi.org/10.1103/PhysRevLett.129.252301
[103] D. Molnar, P. Huovinen, Dissipative effects from transport and viscous hydrodynamics, J. Phys. G 35 (2008) 104125. arXiv preprint arXiv:0806.1367, https://doi.org/10.1088/0954-3899/35/10/104125
[104] H. Song, U.W. Heinz, Multiplicity scaling in ideal and viscous hydrodynamics, Phys. Rev. C 78 (2008) 024902. arXiv preprint arXiv:0805.1756, https://doi.org/10.1103/PhysRevC.78.024902
[105] A. Dimri, S. Bhatta, J. Jia, Impact of nuclear shape fluctuations in high-energy heavy ion collisions, Eur. Phys. J. A 59 (3) (2023) 45. arXiv preprint arXiv:2301.03556, https://doi.org/10.1140/epja/s10050-023-00965-1
[106] P. Möller, A.J. Sierk, T. Ichikawa, H. Sagawa, Nuclear ground-state masses and deformations: FRDM(2012), Atom. Data Nucl. Data Tabl. 109–110 (2016) 1–204. arXiv preprint arXiv:1508.06294, https://doi.org/10.1016/j.adt.2015.10.002
[107] G. Giacalone, J. Noronha-Hostler, M. Luzum, J.-Y. Ollitrault, Hydrodynamic predictions for 5.44 TeV Xe + Xe collisions, Phys. Rev. C 97 (3) (2018) 034904. arXiv preprint arXiv:1711.08499, https://doi.org/10.1103/PhysRevC.97.034904
[108] B.H. Alver, C. Gombeaud, M. Luzum, J.-Y. Ollitrault, Triangular flow in hydrodynamics and transport theory, Phys. Rev. C 82 (2010) 034913. arXiv preprint arXiv:1007.5469, https://doi.org/10.1103/PhysRevC.82.034913
[109] S. Acharya, et al., ALICE, ALICE physics projections for a short oxygen-beam run at the LHC (2021). https://cds.cern.ch/record/2765973. arXiv preprint arXiv:ALICE-PUBLIC-2021-004
[110] C. Zhang, J. Chen, G. Giacalone, S. Huang, J. Jia, Y.-G. Ma, *Ab-initio* Nucleon-nucleon correlations and their impact on high energy ^{16}O + ^{16}O collisions (2024). arXiv preprint arXiv:2404.08385
[111] Y. Wang, S. Zhao, B. Cao, H.-j. Xu, H. Song, Exploring the compactness of α clusters in O16 nuclei with relativistic O16 + O16 collisions, Phys. Rev. C 109 (5) (2024) L051904. arXiv preprint arXiv:2401.15723, https://doi.org/10.1103/PhysRevC.109.L051904
[112] B. Bally, et al., Imaging the initial condition of heavy-ion collisions and nuclear structure across the nuclide chart (2022). arXiv preprint arXiv:2209.11042